Mechanical Properties of Graphene

Y.W. Sun,[1, a)] D.G. Papageorgiou,[1, b)] C.J. Humphreys,[1, c)] D.J. Dunstan,[2, d)] P. Puech,[3, e)] J.E. Proctor,[4, f)] C. Bousige,[5, g)] D. Machon,[6, h)] and A. San Miguel[6, i)]

[1)] *School of Engineering and Materials Science, Queen Mary University of London, London E1 4NS, United Kingdom*

[2)] *School of Physics and Astronomy, Queen Mary University of London, London E1 4NS, United Kingdom*

[3)] *CEMES/CNRS UPR8011, University of Toulouse, F-31055 Toulouse, France*

[4)] *School of Science, Engineering and Environment, University of Salford, Manchester M5 4WT, United Kingdom*

[5)] *Laboratoire des Multimatériaux et Interfaces, UMR CNRS 5615, Univ. Lyon, Université Claude Bernard Lyon 1, F-69622 Villeurbanne, France*

[6)] *Université de Lyon, F-69000 Lyon, France and Institut Lumière Matière, CNRS, UMR 5306, Université Lyon 1, F-69622 Villeurbanne, France*

(Dated: 11 March 2021)

The mechanical properties of graphene are reviewed with particular attention to what is established and what is still uncertain. The thickness and the elastic constants are clarified, and by considering also phonon frequencies it is argued that "best values" come from graphite, when available. Properties not available from graphite include the bending stiffness; this can be determined from studies of carbon nanotubes as well as graphene. In many ways nanotubes provide access to fundamental properties of graphene, not least as they are the only form of graphene that can be unsupported (unstrained) in vacuum. Environmental effects are considered, both interactions with substrates and with other solid and liquid media which may affect the geometrical parameters defining graphene and associated elastic constant. Major uncertainties persist whether slipping or sticking dominates experimental observation, both between graphene and solid media, and between the layers of bilayer and multilayer graphene. The paper concludes with a short discussion of continuum and atomistic models of graphene.

[a)] yiwei.sun@qmul.ac.uk
[b)] d.papageorgiou@qmul.ac.uk
[c)] c.humphreys@qmul.ac.uk
[d)] d.dunstan@qmul.ac.uk
[e)] pascal.puech@cemes.fr
[f)] j.e.proctor@salford.ac.uk
[g)] colin.bousige@univ-lyon1.fr
[h)] denis.machon@univ-lyon1.fr
[i)] alfonso.san-miguel@univ-lyon1.fr

CONTENTS

I. INTRODUCTION

Graphene has attracted enormous attention (*e.g.* the 2010 Nobel Prize) and research effort, because of its extraordinary properties, not the least of which is its two-dimensional (2D) nature. While many layered materials such as graphite and MoS_2 were already known, graphene was the first material in which all the atoms are in a single plane – so for theoreticians, at least, who may ignore the electrons and consider the carbon nuclei as point masses, it is a genuinely 2D material. Yet it is also a very familiar material. It is the material that in stacks of millions or billions of layers, constitutes graphite, much as many sheets of paper make a book.

There are many excellent review articles that cover the mechanical properties of graphene, both experimental and theoretical, and which to be comprehensive have to have about 500 references.[1–3] Why another? Our purpose is different. We aim to clarify points that are often confused in the literature, and where we deem appropriate to identify problems that are as yet unsolved. Some properties of graphene are just what one might expect, given what we know of graphite. Here we review primarily the accuracy to which this is known. Second, some properties are expected to be different, for reasons that are understood. Third, and perhaps most interesting, are the anomalies. By this, we mean the behaviours of graphene that are well-established experimentally, yet which lack adequate explanation according to our current understanding.

An interesting question is "to which extent is the continuum mechanics view applicable to graphene?" Of course, this leads to the definition of a thickness for graphene, which is comparable to trying to define the thickness of an atom. The quantum nature of matter, predominant at this scale, will obviously only lead to an approximate or to a probabilistic answer.

II. BASIC PROPERTIES

The most basic properties determining the mechanical behaviour of a piece of a material are its physical dimensions and its elastic moduli. But how can we define or measure these mechanical properties of graphene? This apparently naive question arises from the fact that the one-atom-thick character of graphene challenges the science of the mechanics

of materials, a discipline based on continuum mechanics and which has developed its successful non-atomistic view since the publication of the first book addressing the strength of materials, "Two New Sciences", written by Galileo Galilei in 1638.[4] Of course, the discipline has subsequently integrated the atomistic nature of materials into its thinking, as in the concepts of theoretical strength and of dislocations, and in the use of molecular dynamics (MD) and density-functional (DFT) modelling.

From the material mechanics point of view, a large part of the challenge of graphene mechanics arises from the ambiguities of defining the thickness of a structure – here a one-atom-thick surface. From this point of view, it is important to recognise that thickness is not a material property, but a property of a structure, such as a plate. Moreover, even a simple structure such as a corrugated-iron roofing sheet has more than one property equally deserving of being called the thickness – maybe the 0.5 mm thickness of the sheet, maybe the 30 mm depth of the corrugations. So the issue is not to define what the thickness of graphene is, but to be clear what the context is and how the concept of thickness enters in, in each context. If one wants to stack n corrugated-iron sheets at random angles, the height of a stack of n sheets will be $30 \times n$ mm, while if they are aligned, the stack will be $0.5 \times n$ mm high. So graphene in AB stacking as in graphite has a thickness of 3.35 Å, unambiguously. We should not be surprised if this value changes for other stackings[5] (*e.g.* around 3.6 Å for random-angle stacking called turbostratic, and see Table I for some graphene thicknesses as described by the distances from various substrates). Nevertheless, while the stacking of corrugated-iron sheets may have no bearing on the physical characteristics of the individual sheets, this can be a totally different issue for graphene. Depending on the geometrical arrangements, modifications of the electronic structure of the individual graphene sheets could be significant.

A. Thickness of graphene

The thickness of graphene is a vexed question. The common description of graphene as a 2D material implies extension in two dimensions but not in the third (*i.e.* zero thickness). Indeed, the very definition of the thickness of graphene is complicated from a quantum mechanics point of view, as it pertains to defining the diameter of atoms. The Yakobson paradox[6] arose through the attribution of values as low as 0.6 Å to the thickness – and hence

Young's moduli as high as 5 TPa. It is interesting to see how the similar issue of the size of atoms was addressed a century ago.

Sir William Bragg proposed the hypothesis that atoms of a given element could be considered to be spheres with a fixed radius.[7] However, the crystal structures of some metals and compounds led to proposals that some atoms have lower symmetry than spherical.[8] Wyckoff re-examined the question and concluded that the hypothesis of constant radii (or other shapes with fixed sizes) must be rejected but that the evidence supported atomic radii that vary more or less according to their environment.[9] This is the basis of the modern view. Modern data compilations give for example the covalent radius of the carbon atom as 0.70 Å. More precisely, the covalent radius of carbon is largest for single-bonded carbon with the C-C bonds in ethane and diamond both at 1.54 Å, smaller for sp^2-bonded (graphite at 1.42 Å and ethene at 1.33 Å bond length) and smallest for triple-bonded carbon (acetylene, 1.20 Å). On the other hand, the van der Waals (vdW) radius of a carbon atom is given as 1.70 Å. An early measurement of the thickness of the benzene molecule gave 4.70 Å,[10] while the thickness of the larger pyrene molecule is 3.53 Å,[11] very close to the spacing of the graphene sheets in graphite at 3.35 Å.

These considerations appear to give a clear meaning to the concept of the vdW thickness of graphene, as much as of simpler molecules such as benzene and the higher polycyclic aromatic compounds such as pyrene. It expresses the distance of closest approach of other physisorbed atoms – whether carbon or anything else, because the repulsive interatomic potential deriving from Pauli exclusion is largely independent of the nature of the interacting atoms, and in the absence of a chemical bond, so is the vdW attractive potential. Following Wyckoff,[9] the thickness should be expected to vary with the environment, whether it is a surrounding gas or a substrate, as can be seen in Table I – even quite considerably as the vdW forces, while always weak, can vary by an order of magnitude.

B. Graphene elastic stiffness tensor

Only in graphite is graphene found in a symmetrical environment (sandwiched between graphene sheets with only a vdW potential binding them) and with a known thickness. We may then define the graphene elastic stiffness constants c_{ij} in this situation as a reference system. To deal with possible variations in thickness in other environments, it makes sense

TABLE I. Experimental graphene-substrate distance for various substrates.

Substrate	Distance [Å]
Ir(111)[12]	3.38
Graphite	3.35
Pt(111)[13]	3.30
SiC(0001)[14]	3.24
Ru(0001)[15]	2.2
Co(0001)[16]	2.2
Ni(111)[17,18]	2.1

to define the in-plane 2D elastic stiffness tensor $c_{ij}^{2D} = c_{ij} d_0$ with $i, j = 1, 2$, and d_0 is the graphite interlayer spacing at ambient pressure. This tensor comes simply from the sp^2 bond bending and stretching stiffnesses, and so is independent of the graphene thickness d *per se*. To see this, consider making the graphene layers in graphite thinner, spaced more closely and reducing a_{33}, as happens under pressure. Then there are more graphene layers per unit volume, a_{33}^{-1}, and the 3D constants c_{11} and c_{12} are increased proportionately – leaving c_{ij}^{2D} unchanged. The out-of-plane elastic constants, particularly c_{33} but also c_{13}, have to be considered separately. This is done in Sec. III C.

A crucial aspect is then to know if the graphene sp^2 bonds – which largely determine c_{ij}^{2D} – are significantly influenced either by the environment of the graphene (what it is in contact with) or by its geometry (for example, bending) leading to a modification of the reference elastic stiffness constants. The zeroth-order approximation would be that there are no such influences. But if there are, we will need also to consider what are the limits in such modifications which can be admitted before saying that we are dealing with a new system. These issues are addressed in Sec. VI.

III. GRAPHENE REFERENCE MECHANICAL PROPERTIES

A. Graphite 3D mechanical properties

Graphite consists of a macroscopic multilayer stack of graphene layers, held apart by the π-orbitals and Pauli exclusion, and held together by the vdW interaction, with a spacing of

3.35 Å.[19] It is, consequently, highly anisotropic, while being isotropic in-plane. The elastic moduli reported in Table II were obtained from inelastic X-ray scattering,[20] but similar values were reported from ultrasonic and static mechanical testing.[21]

TABLE II. Elastic moduli values obtained from inelastic X-ray scattering[20] in Voigt notation

	c_{ij} [GPa]	c_{ij}^{2D} [Nm^{-1}]
c_{11}	1109 ± 16	372 ± 5
c_{33}	38.7 ± 0.7	
c_{12}	139 ± 36	47 ± 12
c_{13}	0 ± 3	
c_{44}	5 ± 0.3	
c_{66}	485 ± 10	
Y	1092 ± 18	362 ± 27
ν	0.125 ± 0.033	(no units)

Within experimental error, the c_{13} of graphite may be negative – and DFT calculations support this.[22] While DFT may not evaluate the interlayer spacing accurately without vdW correction,[23] the related elastic constant c_{33} calculated at the experimental equilibrium spacing agrees well with the experimental c_{33}. That improves confidence in the reliability of the negative calculated value of c_{13}.[22] If c_{13} is truly negative, it might be due to ripples in the measured graphite sample, like what happens with auxetics, prominent structures that have negative Poisson's ratio.[24] This could be further linked to the negative thermal expansion of graphene, which will be discussed later. In a general 3D anisotropic medium, the Young's moduli for a stress σ_{11} are given by more complicated expressions than the usual $Y = c_{11} - 2c_{12}^2/(c_{11} + c_{12})$. The small or vanishing value of c_{13} simplifies this to $Y = c_{11} - c_{12}^2/c_{11}$ for the in-plane Young's modulus of graphene. Similarly the in-plane Poisson's ratio simplifies to $\nu = c_{12}/c_{11}$.

B. In-plane graphene mechanical properties

Under the hypothesis that graphene can be treated as a continuous elastic medium, it is thus expected to have the 3D values given in Table II and hence the c_{ij}^{2D} values also

given there. Indeed, the in-plane Young's modulus $Y^{2D} = 362$ Nm^{-1} is consistent with the $Y^{2D} = 340 \pm 50$ Nm^{-1} of monolayer freestanding graphene measured by atomic force microscopy (AFM)[25], which will be discussed in Sec. IV A.

For graphene in vacuum, the greatest difference from graphite is likely to be an increase in the thickness, as the π-orbitals are no longer compressed by the vdW attractive force – indeed, as discussed above, the thickness becomes defined by whatever convention is used to specify where the π-orbitals end. The 3D elastic constants will vary inversely with the thickness. The 2D elastic constants are unaffected. Neglecting any small effect on the sp^2 bond strength caused by the relaxation of the π-orbitals, and any small contribution of the π-bonds to c_{11} and c_{12}, the 2D elastic constants will be unchanged; they are mostly determined by the carbon sp^2-network.[26]

Direct experimental determinations of the in-plane elastic constants of graphene are much less accurate than those of graphite, but are generally consistent with them within experimental uncertainty (see Sec. IV). The results of *ab initio* theoretical calculations also show very similar in-plane elastic constants of graphene to graphite, with the caveat that it is much harder to assess the uncertainty of these calculations than to assess experimental uncertainties.[22]

Given the large uncertainties on experimental determinations of c_{ij}^{2D} in graphene, the best information about possible perturbations of the in-plane sp^2 bonding comes from a comparison of the phonon frequencies, and in particular the zone-centre E_{2g} optical phonon. It is a Raman active mode, named the G-mode (G for graphite), at about 1600 cm^{-1} in all sp^2-bonded forms of carbon.[27] In graphite, the frequency of the G-mode is at 1575 – 1580 cm^{-1},[27–30] and it is reported at 1581 – 1592 cm^{-1} in graphene.[31–34] This difference of about 0.5% puts an upper limit of about 1% on any change in the stiffness of the sp^2 bonds or c_{ij}^{2D} in going from graphite to graphene.

Chemical perturbations such as substitutional doping and doping by charge transfer from a substrate or nitric acid, etc, mechanical perturbations such as bending, stretching or high pressure, or structural perturbations such as stacking order, again scarcely perturb the GM frequency relative to graphite, a few tens of cm^{-1} at most. The sp^2 covalent bonding is clearly robust. This is actually true of small molecules generally, which like graphene are "all surface", yet whose vibrational frequencies are little affected from the vapour phase, through solvation or liquefaction, to crystalline solid forms. It is not surprising, then, that

this is so for graphene. Of course, the concept of a material that is all surface is not novel; chemistry deals largely with such things. Some readers might be alerted here that shift of tens of cm^{-1} in the G-mode could be considered to be huge in specific studies, but when considering the corresponding change in the in-plane stiffness, such shifts are still very little compared to the large experimental uncertainties from the direct measurements on graphene by AFM (Sec. IV A).

We conclude that graphene and graphite are the same regarding in-plane stiffness within experimental uncertainty, from the G-mode frequency. More details about the G-mode frequency, such as the contributions from the deformed π-orbitals and up to the fifth nearest neighbour C atoms, will be discussed in Sec. VI C and VIII, respectively.

C. Out-of-plane stiffness of graphene

On the assumption that graphene has the vdW thickness equal to the interlayer spacing of graphite (Sec. II A), we may suppose that it has a stiffness in that direction, equal to that of graphite, 38.7 ± 0.7 GPa.[20] This basic assumption is challenged by various objections. For example, in graphite, c_{33} probes the interlayer potentials defined through the π-orbital interaction in an AB stacking. What sense does this make when considering graphene in vacuum or in a solid or liquid molecular environment? Deformation of solids is usually described in terms of the changes in the distances between atoms, measured from nuclei to nuclei, or in crystals, by the spacing of planes of atomic nuclei. It could be argued that with only one plane of atoms, one plane of nuclei, out-of-plane deformation or strain of graphene is meaningless, and with that, the c_{33} of graphene is a meaningless concept.

Against these challenges, thickness and stiffness certainly exist in monolayer graphene, just as atomic radii exist (Sec. II A), and vary with pressure, which defines an atomic radial stiffness. Electronic orbitals extend out of the plane of graphene nuclei and they resist compression. Such resistance (more accurately, compliance) consists of two parts. One is the Pauli exclusion compliance from the overlap of the π-orbitals of graphene and the outer orbitals of the medium that applies compression. It naturally depends on what that medium is and how it is stacked onto graphene. Moreover, the compliance has to be apportioned between the compliance of the graphene and the compliance of the medium. Surprisingly, even if the compressing medium is another graphene monolayer AB-stacked to it, the out-

of-plane stiffness is calculated to be, not that of graphite, but only about half of it.[35] This softness is attributed to the squeezing of π-orbitals through the graphene plane in a bilayer system, whereas such squeezing-through is prohibited in graphite (infinite number of layers) by symmetry.[35] In addition to the compliance of the Pauli exclusion for undeformed π-orbitals, the other contribution from the graphene to the total compliance is from the deformation of the π-orbitals of the graphene. This could be estimated by calculating the energy difference between relaxed and deformed π-electron distributions.

In the absence of a conventionally-defined elastic constant c_{33} based on internuclear distances, one approach to define the out-of-plane stiffness of graphene is to use a related quantity that is itself unambiguously defined and measurable. The in-plane bonds stiffen under compressive in-plane strain, which can be expressed as a 2D strain and converted to a 2D stress by c_{ij}^{2D}. That has been measured by the increase in G-mode phonon frequency under pressure.[31,34,36–38] In graphene as in graphite, the 2D in-plane stress can be applied by hydrostatic pressure, and the 2D stress is then directly proportional to the thickness. Since graphite and graphene are very soft out-of-plane, under hydrostatic pressure the thickness decreases significantly (the π-orbitals being considerably compressed). That gives a large reduction of in-plane force below the linear proportionality with pressure, and therefore a substanially sublinear shift of the G-mode frequency with pressure.[39] An experiment adopting this approach had large experimental uncertainties, but within experimental uncertainty first confirmed from the shift-rate of the G-mode that the thickness of graphene is not significantly different from its thickness in graphite. Then the sublinearity of the shift-rate could not distinguish the graphene $c_{33} = 0 \pm 300$ GPa[40] from graphite (38.7 ± 0.7 GPa).[20] Of course, there are also possible effects of the pressure medium on the graphene response; these are discussed further in Sec. VI below.

D. Properties not related to graphite

In contrast to the foregoing, there are some properties of graphene that are quite distinct from, or unrelated to, any properties of graphite. It is probably accurate to say that these are all properties related to the freedom graphene has to displace in the z-direction, out of plane, in ways that are unavailable to the layers in graphite. Briefly, these include the theoretical instability of a 2D sheet, the negative thermal expansion in-plane of graphene,

and the stiffness in bending of monolayer graphene and of multilayer graphene.

1. Acoustic phonons in graphene; their effect on the thermal expansion and stability of graphene samples

In this section, and the following sections III D 2 to III D 4, we will review the nature of the acoustic phonon modes in graphene. They are responsible for some key properties of graphene: The observation of a negative thermal expansion coefficient under certain conditions, lack of mechanical stability and – in consequence of this – static ripples in the graphene monolayer. These properties reflect, in a fundamental way, the 2D nature of graphene: The lack of restoring forces from adjacent atomic layers in the out-of-plane direction, and the density of states for a 2D material varying in proportion to k rather than k^2.

To begin, we must briefly review the low-energy part of the phonon dispersion relation of graphene. The dispersion relation has been studied for decades prior to the discovery of graphene, as a simplified model for the phonons in graphite.[41–43] Initially these calculations were performed using traditional semi-classical "ball and spring" force constant models, and the results obtained nowadays using DFT calculations[22] are in reasonably good agreement with those obtained previously using "pencil-and-paper" methods. Agreement is also good with the experimental data obtained on graphite using electron energy loss spectroscopy,[44] inelastic neutron[42] and X-ray scattering.[26] Fig. 1 shows the low-energy part of the dispersion relation, calculated in Ref. 22 using DFT. In this section we shall regard low energy as up to 50 meV since we are interested in the phonons which can be excited in significant number by thermal energy at $T \leq 300$ K. (At 300 K, $k_B T \approx 25$ meV).

2. Mechanical stability of graphene

As shown in Fig. 1, there are three acoustic phonon modes which can be excited at 300 K. They are longitudinal (LA) and transverse (TA) polarization in-plane modes (both with linear dispersion relations in the low k limit) and a transverse polarization out-of-plane mode (ZA) with a quadratic dispersion relation in the low k limit ($E \propto k^2$).[22,43] The softness of this mode relative to the LA and TA modes is believed to be partially due to the lack of

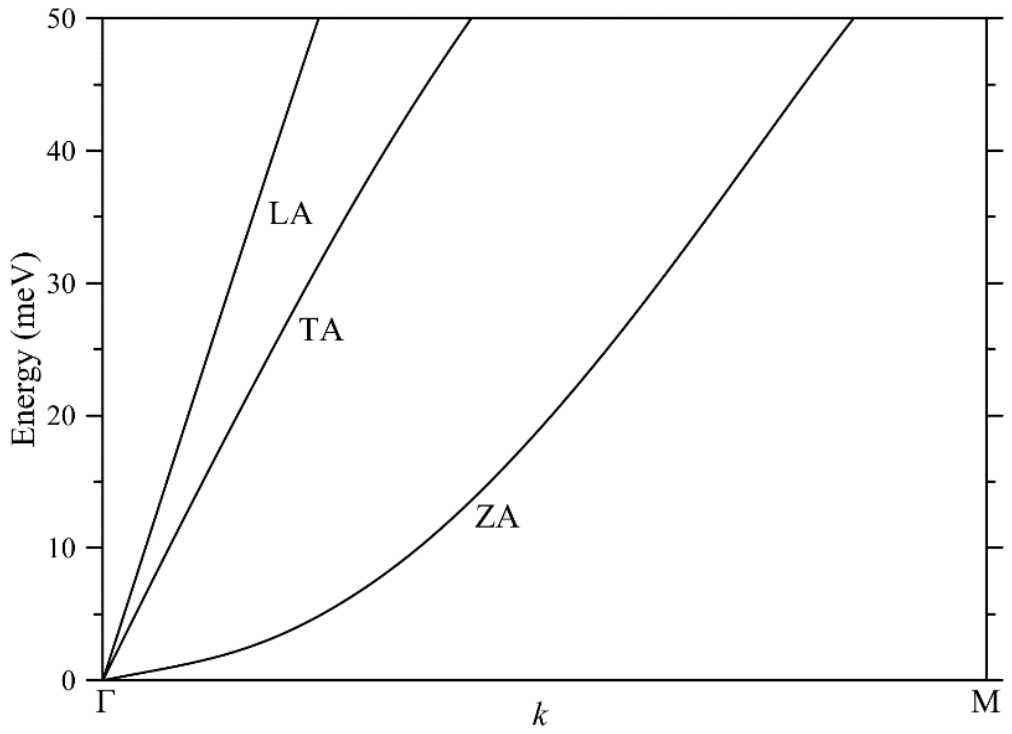

FIG. 1. Low-energy graphene phonon modes along the Γ-M direction in the first Brillouin zone, obtained in Ref. 22 using DFT. LA and TA modes are the longitudinal and transverse polarization in-plane modes and the ZA mode is the transverse polarization out-of-plane mode.

bending stiffness of graphene. However, the low bending stiffness is not necessary to explain the quadratic dispersion relation. A transverse wave on a string (or sheet) with zero tension but a bending stiffness D has $\omega(k) = k^2(D/\rho)^{1/2}$, so the quadratic dispersion relation is fully consistent with the recently measured 1.7 eV bending stiffness of graphene.[39,45] The number of phonons present at temperature T from branch i of the dispersion relation (hence with energy $E_i(k)$) is obtained by multiplying the Bose-Einstein distribution by the density of states $D(k)$ and integrating over all available k (Eq. 1). The lower limit k_{min} corresponds to the longest wavelength mode that can exist on the graphene sheet. So $k_{min} \approx 2\pi/L$ where L is the diameter of the graphene sheet. For macroscopic graphene samples therefore $k_{min} \to 0$ is a reasonable approximation. Referring to Fig. 1 and the known graphene reciprocal lattice, the path $\Gamma \to M$ in reciprocal space covers a range of 2.3×10^9 m^{-1}, whilst $k_{min} \approx 10^5$ m^{-1} for a 10 μm diameter graphene sheet.

The upper limit k_{max} should be set so as to integrate over all possible phonon modes, in reality the upper limit of the integral is set by the Bose-Einstein distribution term dropping

to zero upon increasing k, E.

$$N = \int_{k_{min}}^{k_{max}} \frac{1}{e^{\beta E(k)} - 1} D(k) dk \tag{1}$$

Here, we write $\beta = 1/k_B T$ for convenience. The densities of states in 1D, 2D and 3D systems, per unit area/volume, are given by:

$$\begin{aligned} D_{1D} &= \frac{1}{\pi} \\ D_{2D} &= \frac{k}{2\pi} \\ D_{3D} &= \frac{k^2}{2\pi^2} \end{aligned} \tag{2}$$

It has been shown that the value of the integral in Eq. 1 diverges to $+\infty$ when a 2D density of states function is utilized, combined with a quadratic dispersion relation.[46] This is due to the value of the integrand diverging in the low-k limit. The experimental observations that genuinely free-standing graphene sheets do not exist, and that all graphene sheets are covered in static ripples (so, in at least one respect, not genuinely 2D) are attributed to this divergence.[46,47] In addition, this divergence prevents the categorization of free-standing graphene sheets as a metastable form of carbon in an equivalent manner to diamond, nanotubes and fullerenes at ambient conditions.

In this section, we are going to explore the cause of this divergence in a little more detail – can it be observed in systems with other dimensionalities, and with other dispersion relations? In Table III we give the integrands that would be utilized in Eq. 1 for phonon modes with quadratic and linear dispersion relations for 1D, 2D and 3D systems. Since we seek only to evaluate which of these integrands diverge we have assumed a finite non-zero temperature and omitted all constant terms, where we assume β is a finite constant since $T > 0$ K. The integrands are evaluated in the low-k limit (equivalent to assuming that the sample is large enough to support phonons across essentially the entire Brillouin zone) using first order expansions of the exponential term ($e^x \approx 1 + \mathrm{x}$), appropriate since we are considering exclusively acoustic phonons for which $E \to 0$ also in the low-k limit.

Summarising the findings from Table III, we observe that in a 3D system divergence is not observed for a linear or quadratic dispersion relation, for a 2D system divergence is observed only with a quadratic dispersion relation, and for a 1D system divergence is observed with either a linear or quadratic dispersion relation. These differences are due to the density of states function being different in each case.

TABLE III. Integrands $I_k^{(n)}$ to evaluate the number of phonons present at finite temperature for different dispersion relations, in systems with different dimensionality n. Constant terms and temperature dependence have been omitted.

	1D	2D	3D
$E \propto k$	$I_k^{(1)} = \frac{1}{e^k - 1}$ $\lim_{k\to 0} I_k^{(1)} = \frac{1}{k}$	$I_k^{(2)} = \frac{k}{e^k - 1}$ $\lim_{k\to 0} I_k^{(2)} = 1$	$I_k^{(3)} = \frac{k^2}{e^k - 1}$ $\lim_{k\to 0} I_k^{(3)} = k$
$E \propto k^2$	$I_{k^2}^{(1)} = \frac{1}{e^{k^2} - 1}$ $\lim_{k\to 0} I_{k^2}^{(1)} = \frac{1}{k^2}$	$I_{k^2}^{(2)} = \frac{k}{e^{k^2} - 1}$ $\lim_{k\to 0} I_{k^2}^{(2)} = \frac{1}{k}$	$I_{k^2}^{(3)} = \frac{k^2}{e^{k^2} - 1}$ $\lim_{k\to 0} I_{k^2}^{(3)} = 1$

To our knowledge, the consequences of this divergence have not been studied experimentally in 1D systems. Certainly its observation would require the existence of an extremely long system to ensure $k_{min} \to 0$, and for the system to be free-standing to allow these phonons to propagate. The nearest humankind has got to a genuinely 1D system is carbyne – in recent years carbyne chains up to 600 nm in length have been synthesized, satisfying the first condition.[48] But the requirement that they are enclosed inside a carbon nanotube probably prevents the second condition from being satisfied. Single-walled carbon nanotubes (SWCNTs) themselves are not strictly one-dimensional as far as the density of states function is concerned. The quantization condition for the direction along the tube axis is the requirement for a standing wave with allowed wavelengths determined by the tube length, whilst the quantization condition for the direction tangential to the tube axis is for travelling waves with allowed wavelengths determined by the tube circumference. Thus, whilst the allowed quantum states are far more widely spaced in the tangential direction, the electron and phonon wavevectors do still have 2 degrees of freedom, and the density of states function should follow a 2D form rather than the 1D form.

As far as graphene is concerned, the divergence in the number of out-of-plane phonons at finite temperature is believed to be responsible for the following experimental observations. Firstly, real monolayer graphene samples can only exist when provided with some mechanical support. Usually this is provided by a substrate. Samples may be described in the literature as "freestanding" when there is an aperture in the substrate or some similar arrangement, but there is always some mechanical support. Monolayer graphene samples may be suspended in a liquid such as water, in which the viscosity of the liquid provides adequate support.[47,49]

Secondly, real monolayer graphene samples are always rippled. These ripples are expected from the findings of atomistic simulations.[50] They have been observed using electron diffraction[51] and also scanning tunnelling microscopy,[52] which has confirmed that they are static ripples, with $\lambda \approx 5$ nm. The ripples become weaker for progressively thicker graphene samples as the thickness of the graphene sample itself provides the required rigidity. These ripples are a completely separate effect to the Brownian motion observed in graphene.[53,54]

The role of ripples in ensuring stability can be understood in terms of the restoring forces. The softness of the ZA mode shown in Fig. 1, compared to the in-plane modes, is because of the lack of restoring forces due to bond-stretching in the low amplitude limit, and of those due to bending in the large-wavelength limit. The curvature induced by the ripples ensures that there is some restoring force due to bond-stretching even in the low amplitude limit, making the mode — partially – analogous to the radial breathing mode in SWCNTs.[55]

3. Thermal expansion coefficient of graphene

The existence of thermal expansion is perhaps the most intuitive example of the interplay between static and dynamic material properties. The lattice constant of a solid is considered the archetypal static property, yet at $T > 0$ K it is altered (usually increased) by the presence of phonons; the archetypal dynamic property. The observation that the vast majority of materials expand upon heating is a consequence of the nature of the function $V(r)$ giving the potential energy between two of the atoms comprising the solid as a function of their separation r. The Lennard-Jones potential is frequently utilized as a good approximation for covalently bonded solids even though it is only strictly correct for solids where the cohesion is due solely to vdW forces. In any case, the potential will always have three key features in common with the Lennard-Jones potential: (1) It will be attractive for moderate values of r, with a minimum at $r = r_0$, the inter-atomic separation in the absence of phonon effects. (2) In the limit $r \to \infty$, $V \to 0$. (3) In the limit $r \to 0$, $V \to +\infty$ to prevent atomic overlap. As a result of these features, $V(r)$ is not symmetric about $r = r_0$ and this asymmetry will, in the absence of other effects, favour thermal expansion rather than contraction.

This argument applies directly to any reasonably isotropic and dense 3D solid and, for that matter, a 2D solid existing in a 2D world (in which case out-of-plane phonon modes would not exist). However, graphene's position is as that of a 2D solid in a 3D world. In

this case, the excitation of an out-of-plane vibration does not cause any thermal expansion in the out-of-plane direction. However it can cause contraction in the in-plane direction as atoms are pulled inwards by the out-of-plane movement.

Thus, for graphene to exhibit a negative coefficient of thermal expansion coefficient (CTE), all that is necessary is for the contribution from the out-of-plane phonons to dominate over that from the in-plane phonons. We can see how this can be the case at low temperature from Fig. 1. The quantum states available for all phonons are equally spaced in k-space so, when phonons of all kinds (LA, TA, ZA) can be excited up to a certain energy, the out-of-plane ZA phonons dominate as they cover a wider area of k-space. The qualitative arguments proposed here are borne out by the findings of detailed theoretical calculations;[22] Graphene should indeed exhibit a negative CTE.

However, as shown earlier a graphene sheet which is genuinely freestanding, and therefore free to expand and contract, cannot exist. Experimental measurements of the CTE of graphene are therefore indirect and prone to large experimental, theoretical and conceptual uncertainties.[56] Most commonly, it has been measured by varying temperature whilst the graphene is adhered to a substrate. The graphene is assumed to adhere perfectly to the substrate due to its extremely high surface area to volume ratio so, upon temperature increase the graphene would be forced to expand rather than contract and is therefore under significant tensile strain. The extent of this strain is usually calculated using Raman measurements on the G peak,[57] though grazing incidence X-ray diffraction has also been utilized.[58] Potential sources of uncertainty in such experiments include, but are not limited to:

- The logic of such experiments is often not clearly presented. When a thin film fully adheres to a substrate, the difference in thermal expansions causes a stress in the film, not a strain. Stress cannot be measured by Raman. The CTE of the film should be directly measured by Raman of the thermal strain in a *free-standing* specimen of the film. Then to correct for the temperature effect on the phonon frequency, the phonon shift at known strain and ambient temperature is compared with the data from the film adhering to a substrate, at a known strain and elevated temperature. Given the difficulty of studying free-standing graphene, data from theoretical simulations is commonly used instead.

- Commonly used substrates for graphene consist of layers of different materials with different TEC. It is not always clear which layer dominates, and to what extent the layers remain bonded.

- The out-of-plane phonons causing the negative TEC should be suppressed to some extent by the presence of the substrate. It is thus not clear how applicable findings regarding graphene on a substrate are to free-standing graphene.

- We assume a value for the Grüneisen parameter (for the phonon responsible for the G peak) when the strain is calculated from the G peak Raman measurement.

- Graphene does not always adhere perfectly to the substrate.

Notwithstanding these problems, the experimental evidence is consistent with graphene having a negative TEC at temperatures up to at least 500 K.[56] (and references therein) This is also the case for the in-plane measurements on graphite. Indeed, comparing reported values and uncertainties of the TEC for graphene and for graphite in-plane,[22,59–61] it is difficult to find any justification for considering them to be different. The small or negative CTE is reflected in the contrasting characteristics of graphene grown by chemical vapour deposition (CVD) and epitaxial growth (EG). Both growth processes take place at high temperature, followed by the substrate contracting upon cooling. In the case of the CVD graphene, Raman measurements at ambient conditions indicate that the graphene has "relaxed" *i.e.* slipped over the substrate upon cooling to stay in equilibrium. However, Raman measurements made on the EG graphene at ambient conditions indicate that it has remained adhered to the substrate upon cooling after growth.[62] As a consequence it is under significant compressive strain; equivalent to several GPa pressure.[56]

As briefly mentioned above, 3D materials with a layered structure can also exhibit a negative thermal expansion coefficient along one axis or in one plane,[63–65] although the phonon modes that cause this will cause positive thermal expansion along some other axes. In graphite at 300 K for example, the in-plane thermal expansion coefficient is *ca.* -1.4×10^{-6} K^{-1}, but the out-of-plane thermal expansion coefficient is *ca.* $+25 \times 10^{-6}$ K^{-1}.[22]

4. *Grüneisen parameters and elastic bands*

The negative thermal expansion coefficient resulting from the ZA mode — by definition — results in this mode having a negative Grüneisen parameter (Grüneisen parameters for all phonon modes in graphene are calculated throughout the first Brillouin zone in Ref. 22). In the Grüneisen approximation, the pressure and temperature dependence of the phonon mode can both be incorporated into the volume or lattice parameter dependence on pressure and temperature, linked by the Grüneisen parameter. For a 2D material such as graphene we can write, following the approach in Ref. 34:

$$\frac{\omega(P,T)}{\omega_0} = \left(\frac{\alpha(P,T)}{\alpha_0}\right)^{-2\gamma_{ZA}} \tag{3}$$

where $\alpha(P,T)$ is the pressure and temperature-dependent lattice parameter, as projected into the basal plane of the graphene lattice. In this case if $\gamma_{ZA} < 0$, $\omega(P,T)$ will decrease under isothermal compressive strain and increase under isothermal tensile strain. Whilst highly unusual on a microscopic level, it is the behaviour we are used to observing in common macroscopic 1D systems in everyday life: When you stretch elastic bands, or guitar strings, or the shrouds and stays of a yacht, they twang at a higher frequency!

5. *Bending stiffness*

In 3D systems, while the elastic constants discussed above are properties of a material, a bending stiffness is a property, not of a material, but of a structure, i.e., related to geometry. It is however defined in a similar way. The elastic constants are the second derivatives of the potential energy with respect to deformation (strain). Graphene has the additional degree of freedom, of bending to a curvature κ ($= 1/R$ where R is the radius of curvature). This additional degree of freedom, bending, and hence a bending stiffness, has no analogue in graphite. To account for the bending stiffness, D, defined by the energy of curvature κ,

$$U = {}^1\!/_2 D\kappa^2 \tag{4}$$

there is a large literature in which an effective Young's modulus Y_{eff} and an effective thickness h_{eff} are introduced such that both the in-plane elastic moduli and the bending stiffness

can be expressed:

$$\begin{aligned} Yh &= Y_{eff}h_{eff} \\ D &= \frac{Y_{eff}h_{eff}^3}{12} \text{ or } \frac{Y_{eff}}{1-\nu^2}\frac{h_{eff}^3}{12} \end{aligned} \tag{5}$$

where in the second expression for D it is the plane-strain modulus that is used, as is correct for a plate made of an isotropic material.

The model of Eq. 5 has had remarkable success in capturing the behaviour of graphene and nanotubes, particularly in contexts where beam, plate and shell theory are used to understand buckling behaviour under load.[6] Due to the uncertainties of a definition of graphene thickness, on the other hand, it has led to claims that nanotubes have "an extremely large Young's modulus",[66] for example the value of 5.5 TPa given by Yakobson *et al.* for Y_{eff}.[6] Similarly, astonishment has been expressed at the small values of h_{eff}, as low as 0.066 nm, "ultrathin compared with the C-C bond length 0.142 nm".[66] The very wide range of values reported for these parameters[67] has been described as a paradox (Yakobson's paradox).[68,69] As some authors have recognised, there is no paradox,[70–72] but much of the literature fails to distinguish h and Y from h_{eff} and Y_{eff}. The wide ranges of values express only the imprecision in the determination of D by different methods. The unphysical values found for Y_{eff} and h_{eff} simply reflected the unphysical nature of these parameters, which correspond to nothing in the real world but are simply convenient ways of representing D in structural engineering computational packages that do not permit D to be entered independently of Y and h (if any such packages exist, which is doubtful, as engineers routinely analyse structures of this sort, such as honeycomb-filled or rib-reinforced plates).

Reported experimental methods of measuring D range from the collapse pressure P_C of nanotubes under high pressure (1.7 ± 0.2 eV),[45] to the taper angle of a strip torn from an adhesive substrate (2.1 ± 0.1 eV).[73] A value of 2 eV was estimated from the phonon dispersion measured by high resolution electron energy loss spectroscopy (HREELS), on Pt (111) supported graphene.[74] Other measurements reported values as high as $10^3 - 10^4$ eV for rippled monolayer[75] and $35.5^{+20.0}_{-15.0}$ eV for bilayer.[76] Torres-Dias *et al.* found that for nanotubes of small diameters, the normalised collapse pressure $P_C R^3 = 3D$ dropped substantially below the theoretical value, which could be due to the softened bending potentials at large bending angles, or an effect of atomicity.[45] Carter *et al.*[77] study the Euler buckling load for a straight pillar. When the compliance of a continuous pillar is concentrated at a few points (atoms,

or angular springs) between rigid portions, the buckling load is substantially reduced. The effect is hard to explain, but is readily derived from the TA phonon dispersion curve of the infinite linear chain, which predicts a decrease of the phase velocity of the TA mode as the wavelength decreases. In any case, this observation requires that the bending stiffness of flat graphene is obtained, as in Ref. 45, from the extrapolation of normalised experimental collapse pressures to $R^{-3} = 0$.[45,77]

6. *Folding*

When a sheet of graphene is folded over onto itself, it adheres due to the vdW interaction. The radius of the fold is determined by the strength of the vdW attraction and by the value of D, and is of the order of the radius of C_{60}. An example is found in large-diameter SWCNTs, which are collapsed already at ambient pressure into the shape called "dogbone" or "peanut". This presents a cavity of ≈ 0.6 nm in diameter at the edge.[78,79] This small diameter reflects the very small value of the bending stiffness of monolayer graphene, in the range of 1 eV, but an accurate evaluation depends on knowing the strength of the vdW adhesion holding the fold folded. The atomic nature of the sheet plays a role, and folding is angle dependent as reported in the study of Zhang *et al.*[80] They reported that graphene sheet tends to fold along armchair (0° folding angle) and zigzag directions (30° folding angle). Consequently the spontaneous collapse of large nanotubes must depend on the chirality, which imposes the folding angle. The most unfavorable direction has the folding angle of 10°. Under very high temperature annealing (2000 °C) the unfavourable angle of folded graphene generates defects such as pentagons, relaxing the stress and leading to an irregular edge composed of zigzag and armchair directions.[81]

For bilayer and multilayer graphene with n layers ($n > 1$), the angle dependance disappears and this cavity size is governed by the number of layers, n. The length of the folding (shape of a pear) is well described by:[82]

$$L(n) = \pi\sqrt{\frac{D}{\gamma}} = \left[\pi\sqrt{\frac{Y}{\gamma}\frac{d_{vdW}^3}{12}}\right] n^{\frac{3}{2}} \tag{6}$$

where D is the bending stiffness of the multilayer per unit length, d_{vdW} is the equilibrium distance between two graphene layers, Y is the Young's modulus, γ surface adhesion energy per unit length around 260 mJ·m^{-2} (42.2 meV/atom).[82] In Chen *et al*,[83] the bending stiffness

D_n(eV) is well fitted by $6.7 \times (nh)^2$ with n between 2 to 6. These results are completely different even if for both relations, the bending stiffness of multilayer graphene is higher than a simple summation of the bending stiffness of each individual layer. The mechanical properties of bilayer and multilayer graphene depend critically on the issue of slipping or binding between layers. If layers slip freely, then the bending stiffness of n-layer graphene will be nD_1 which is not the case from simulation. On the other hand, if slipping does not occur, the bending stiffness of a bilayer, D_2, will be largely unrelated to D_1 as it then derives directly from the in-plane stiffness (plus nD_1).[84] Neglecting D_1 for multilayers, we have $D_2 = 2(h/2)^2 c_{11}^{2D}$, $D_3 = 2h^2 c_{11}^{2D}$ and $D_4 = 2[(3h/2)^2 + (h/2)^2] c_{11}^{2D}$ and for large n, we recover the usual relation: $D_n = \frac{c_{33}}{1-\nu^2} \frac{(nh)^3}{12}$. The numerical values $D_1 = 0.7$, $D_2 = 131$ and $D_4 = 1308$ eV are to be compared to the value of $D_1 = 2.1$, $D_2 = 130$ and $D_4 = 1199$ eV reported by Sen *et al.*[73]

7. *Shearing, sliding and friction between graphene layers*

In multilayer graphene, as mentioned in the previous Section, whether shearing or sliding occurs between layers determines the bending stiffness of the multilayer. In addition, a Raman shear mode is observed at low wavenumbers, between 31 cm^{-1} (bilayer) to 43 cm^{-1} (bulk).[85] Considering a linear chain model, it is possible to define an interlayer coupling stiffness, $\alpha = 12.8 \times 10^{18}$ N·m^{-3}. The same value fits the Raman from bilayer through to graphite. It is a microscopic measure of the shear modulus, $\alpha d_0 = c_{44} = 4.3$ GPa, close to the value of Table I. It corresponds to a spring constant $k = 0.419$ N·m^{-1} for an unit cell. The existence of this mode shows the corrugation of the graphene surface at the atomic scale. It is also possible by friction to characterize atomically the surface. For a monolayer, the presence of ripples can increase the friction by 40% compared to bulk graphite where the layers are flat.[86] The friction results are well reproduced by calculation.[87] Finally, the sliding, corresponding to electrostatic interactions and dispersive forces, and its dependence on atomic direction has been calculated.[87] During the sliding, the interlayer distance changes by 0.04 Å and the force is found to be in the range of 1.92 pN/atom considering no relaxation of the atoms, which is close to the experimental value of 2.11 pN/atom. These values are typical of flat 2D systems (h-BN).[87]

IV. MEASURING GRAPHENE MECHANICAL PROPERTIES

The nanoscale thickness of monolayer graphene makes the accurate measurement of its mechanical properties a challenging task. A number of techniques have been proposed in the literature[88–90] to measure the mechanical properties of graphene membranes. Some of the most important ones are described here.

A. Atomic force microscopy

The use of AFM in the study of the mechanical properties of graphene usually involves suspension of monolayer graphene over a substrate that has been previously patterned with holes and then applying a local force to the surface of graphene with high precision. In this way, the in-plane mechanical properties can be obtained. The work of Lee *et al.*[25] was the first to measure the elastic modulus and fracture strength of graphene by using an AFM tip to indent graphene that was suspended over circular wells. Force-displacement (load-indentation) curves were obtained by indenting the membranes under constant speed. The applied force can then be calculated. However, the exact theory is far from simple[91] and many authors have used equations that appear to be over-simplified. The following equation, for example, has been frequently used,[25]

$$F = \sigma_0^{2D}(\pi R)(\frac{\delta}{R}) + E^{2D}(q^3 R)(\frac{\delta}{R})^3 \tag{7}$$

where R is the radius of the circular well, δ is the indentation depth, σ_0^{2D} is the pre-tension and E^{2D} is the 2D Young's modulus, and q can be expressed as $1/(1.05 - 0.15\nu - 0.16\nu^2)$, where ν is the Poisson's ratio of graphene.[25] Given the uncertainties in the other parameters, one may question the spurious precision implied by the inclusion of the factor q, which ranges only from 0.95 to 1.05 over the whole range of possible values, $0 < \nu < 0.5$, and has the value of 0.98 for the graphene value of $\nu = 0.16$. It is implausible that the contribution of the pre-tension to the force, for a given depth, is independent of the radius of the well. Fitting the data, values of the modulus and fracture strength of graphene are obtained. Similarly, the breaking strength can be calculated from:

$$\sigma_{max} = \left[\frac{F_{max}E^{2D}}{4\pi R_{tip}^2}\right]^2 \tag{8}$$

where R_{tip} is the radius of the AFM tip and F_{max} is the force at which the membrane breaks.

A variation of the AFM nanoindentation method where graphene suspended over a circular hole, is the so-called beam bending method, where the 2D membrane is now in the form of a beam (or a stripe) and is suspended over a trough in the substrate. In this case the load-deformation relationship is:[92]

$$F = \frac{Ew\pi^4}{6}\left(\frac{t}{L}\right)^3\delta + \frac{\sigma_0 w\pi^2}{2}\left(\frac{t}{L}\right)\delta + \frac{Ew\pi^4}{8}\left(\frac{t}{L^3}\right)\delta^3 \tag{9}$$

where w, t, and L are the width, thickness and length of the beam, σ_0 is the intrinsic stress, δ is the beam deflection, F is the load applied in the beam centre and E is the Young's modulus.

Although the majority of the AFM-based results in the literature agree (within large experimental uncertainties) with values estimated from the bulk materials and with theoretical calculations, it has been debated whether AFM nanoindentation can measure the mechanical properties of macroscopic 2D membranes in a meaningful way.[93] The AFM tip focuses on very small areas where the probability of defects is low. Intrinsic defects, ripples and crumples that are known to reduce the inherent properties of a "perfect" material are very common in 2D materials, yet are sometimes ignored or overlooked. Parameters that introduce uncertainties into the interpretation of data include the initial stress of the 2D membranes, the position of the indenter (which needs to be in the exact centre of the membrane) and the indenter radius. Nevertheless, AFM nanoindentation is one of the most popular experimental methods to measure the mechanical properties of 2D membranes and has been used for a number of 2D materials.

Lee *et al.*[25] found the Young's modulus of monolayer graphene to be $E_{2D} = 340 \pm 50$ N m^{-1}, corresponding to $E = 1.0 \pm 0.1$ TPa for a thickness of 3.35 Å. However, not all graphene samples are flat. Nicholl *et al.*[94] and Ruiz-Vargas *et al.*[95] focused on crumpled and wrinkled graphene prepared by CVD and found that the stiffness obtained by AFM nanoindentation was reduced, compared to monocrystalline graphene.

A different, very useful application of AFM nanoindentation was reported by Cui *et al.*[96] They performed a fatigue study using a combination of static and cyclic mechanical loading of a suspended 2D film (Fig. 2 (a)). Monolayer and few-layer graphene survived more than 109 loading cycles at a mean stress of 71 GPa and a stress range of 5.6 GPa; that is higher than any material reported so far.

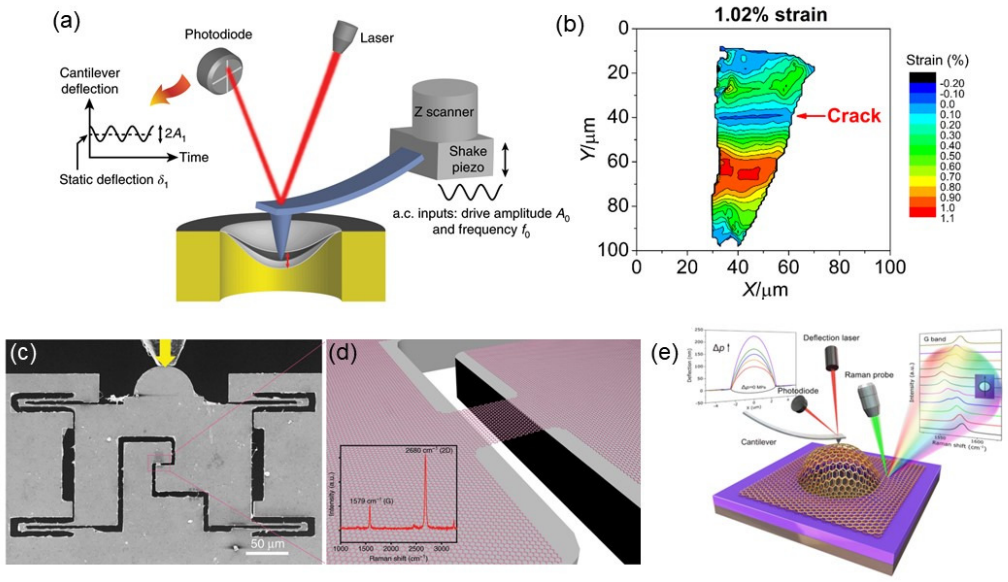

FIG. 2. (a) Schematic of the AFM fatigue testing set-up. Reproduced with permission from Nature Materials **19**, 405 (2020).[96] Copyright (2020) Springer Nature. (b) Strain contour map of a monolayer graphene flaked under 1.02% strain, where the strain distribution can be identified. The presence of a crack running through the upper part of the flake can be realised by the blue 0% strain line. Reproduced from Ref. 97 with permission from The Royal Society of Chemistry. (c) A deposited graphene sample in the centre of a push-to-pull micromechanical device, actuated by an external pico-indenter. The yellow arrow indicates the indentation direction during a tensile testing process. (d) Illustration of the graphene sample suspended between the device gap. (c) and (d) are reproduced from K. Cao, S. Feng, Y. Han, L. Gao, T. Hue Ly, Z. Xu, and Y. Lu, Nature Communications **11**, 284, 2020;[98] licensed under a Creative Commons Attribution (CC BY) license. (e) Schematic diagram of the bilayer graphene balloon. The left inset shows the increasing pressure on a graphene bubble, while the right inset shows the Raman G band of graphene across the balloon (line scan). Reproduced with permission from Phys. Rev. Lett. **119**, 036101 (2017).[99] Copyright (2017) The American Physical Society.

B. Raman spectroscopy

Raman spectroscopy has been used extensively for the study of the mechanical properties of carbon-based materials as a result of their strong resonant Raman scattering. The well-defined characteristic Raman peaks enable the observation of a number of very interesting phenomena and properties under uniaxial or biaxial strain.

For uniaxial strain, these experiments involve the deposition of monolayer or multilayer graphene flexible onto a polymeric substrate, which is subsequently strained by 2-, 3- or 4-point bending under a Raman spectrometer. The application of strain leads to an elongation of the C-C bonds and the lattice deformation is clearly and accurately evidenced by down-shifts of the Raman peaks. Mohiuddin *et al.*[33] first studied the deformation of monolayer graphene deposited onto a flexible substrate under uniaxial tensile strain and found that the shift of the 2D-mode is about -60 ± 5 cm^{-1}/% strain. This downshift corresponds to the material having an elastic modulus in the order of 1 TPa and was subsequently confirmed by a number of research groups.[1,97,100,101] The G band is split by the uniaxial strain into G^+ and G^- peaks. The shift of the G^+ band was -10.8 cm^{-1}/% strain while the shift of the G^- band was -31.7 cm^{-1}/% strain. The frequency of the G-mode is related to the C-C bond stiffness, though it contains non-negligible contribution from up to the fifth nearest neighbour (more details in Sec. VIII).[26] It is nevertheless reasonable to consider that its shift with strain has contribution only from the nearest neighbour, and is therefore determined by the anharmonicity of the C-C bond. The physical meaning of the shift of the 2D-mode is less clear as it is related to the evolution of the LO/TO phonon dispersion under strain.[102]

The strength of monolayer graphene can be also studied by *in situ* Raman mapping. Zhao *et al.*[97] prepared monolayer graphene by mechanical exfoliation, deposited the samples onto polymer substrates and performed *in situ* Raman mapping at different strain levels to obtain the strain distributions over the graphene flakes. Strain contour maps showed significant events such as strain build up, edge effects and cracks which developed with increasing strain (Fig. 2 (b)). Two main mechanisms of failure were observed: flake fracture, and failure of the graphene/polymer interface. Low strengths were observed for these macroscopic monolayer samples, only $10 - 15$ GPa, an order of magnitude lower than the value of 130 GPa that was reported by Lee *et al.*[25] Simulations suggest that this was due to the presence of defects.[97] Under large deformation, Raman observations also suggest a manifestation of

large nanometer-scale strain inhomogeneity within the laser spot size.[103,104]

In multilayer graphene, Gong *et al.*[105] studied the effect of the layer number on the downshift of the 2D band and found that monolayer and bilayer graphene displayed almost the same redshift rate. On the other hand, with further increasing layer number, the shift rate decreases significantly. The 2D Raman profile was fitted by a single Lorentzian, although a broadened 2D profile is expected with increasing number of layers as it contains more components,[102] and the decrease of the 'average' shift rate was interpreted as showing some slippage between the layers, *i.e.* reduced internal stress transfer. However, these spectra were recorded at the centres of the flakes. Similarly to shear lag, slippage between layers or between the lowest layer and the substrate should reduce the strain at the edge of the flake first and propagate inwards as the strain is increased (Fig. 2 (b)). More detailed studies would be desirable.

For biaxial strain, blister testing as described in Sec. IV D below is appropriate. G-mode shifts as large as -80 cm^{-1} are obtained and the deduced Gruneisen parameter of $1.8 \pm 10\%$ is compatible with biaxial strain.[106] The calculated slope (with some approximation on Y, D and d_{vdW}) $\Delta\omega_G/\epsilon = -57$ cm^{-1}/% can be compared with later similar studies. Shin *et al.*[103] achieved biaxial reversible strain up to $\approx 2\%$. Using the same approximations, they found $\Delta\omega_G/\epsilon = -62$ cm^{-1}/%. With large biaxial strain, the linewidth of the G-mode increases.

Interlayer modes, the layer breathing mode and shear mode, are convenient measures of adhesion and shear strength between graphene layers. A linear chain model describes the frequency of the shear mode, and its change with number of graphene layers very well, as discussed in Sec. III D 7. The model applies to the layer breathing mode too.[107] The layer breathing mode becomes Raman-active, when graphene layers are twisted from AB stacking. Its intensity is usually very weak, and requires resonance condition to be observable. Resonance Raman spectroscopy is particularly useful to study graphene and CNTs samples, where the resonance condition is that the energy of the in-coming or out-going laser matches the gap between van Hove singularities in these low-dimensional samples.[108,109]

C. *In situ* tensile tests

For *in-situ* tensile tests, nanomechanical testing devices are usually introduced within a scanning electron microscope (SEM) or transmission electron microscope (TEM) and the

deformation of the graphene is followed in the images. To study its fracture toughness, Zhang *et al.*[110] suspended nanocrystalline graphene over the jaws (gap) of a micromechanical device driven by a nanoindenter, within an SEM chamber. This imposed uniaxial tension on the graphene. Brittle fracture was observed when a central crack had been machined by FIB in the graphene samples prior to testing. The fracture toughness of graphene (important for engineering applications) was found to be $K_c = 4.0 \pm 0.6$ MPa, while the critical strain energy release rate was $G_c = 16 \pm 5$ J·m^{-2} (where we estimate the uncertainty on G_c from their data). Cao *et al.*[98] reported *in situ* tensile tests within an SEM chamber and measured the elastic properties and stretchability of monolayer CVD graphene (Fig. 2 (c,d)). The Young's modulus was ~ 1 TPa, while the tensile strength was around $50 - 60$ GPa, when the elongation of the sample was $\sim 6\%$. Once again the actual strength of macroscopic graphene samples is significantly lower than the value of 130 GPa reported by Lee *et al.*[25] in AFM nanoindentation. Brittle fracture initiated from the edges of the samples, suggesting that control of the edge states and edge effects could lead to greater strength.

In situ TEM can offer useful information on cracks and defects in graphene. For example, Fujihara *et al.*[111] observed that crack propagation takes place along a specific crystallographic direction, in order to create zigzag edges. Kim *et al.*[112] showed that the presence of grain boundaries influences crack growth. When the stress is normal to the grain boundaries, the crack can follow the boundary; however, if the crack is initiated away from the grain boundaries and at some random orientation with respect to it (with the strain direction not normal to the grain boundary), the stiffness the tear experiences is more or less unaffected by the grain boundary and the crack will pass through the grain boundary, switching to the most favourable direction in the next grain.

D. Pressurized blister method

The use of the pressurized blister (bulge, bubble, or balloon) method can provide information on the mechanical properties of 2D membranes and the interfacial adhesion between the substrate and the membrane. For these experiments, graphene is again suspended on top of a hole, or microcavity, in the substrate. The vdW forces between the substrate and the membrane hold the sample in place. Gas is fed in the hole thus pressurising the membrane. This leads to a spherical blister with a radius R. AFM is used to measure the blister

(compare Raman methods in Sec. IV B). The relation between its height, δ, and the pressure difference inside and out, Δp, is,[113]

$$\Delta p = K(\nu)(Ed\delta^3)/R^4 \tag{10}$$

where E is the Young's modulus, and d is the graphene thickness. $K(\nu)$ is a coefficient depending on Poisson's ratio only and is very close to 3. Thus the elastic modulus can be calculated from the measured AFM deflections.

The group of Bunch[114] first measured the adhesion of graphene on a silicon oxide substrate in this way. The adhesion strength is revealed by the pressure at which the blister diameter begins to exceed the hole diameter, i.e. when the graphene begins to peel away from the substrate. The relationship is given by Bodetti *et al* as Eq. 14 of their paper.[115] They obtain adhesion energies of 0.45 $\pm$ 0.02 J/m^2 for monolayer graphene and 0.31 $\pm$ 0.03 J/m^2 for few-layer graphene ($2-5$ sheets). With its high flexibility, graphene, especially monolayer graphene, is able to conform to the topography of very smooth surfaces, thus leading to high values of adhesion energy. However, much lower values may be observed,as adhesion between a graphene sheet and a substrate (or surface) is highly dependent on the surface conditions such as moisture, roughness, chemical reactivity and others and a considerable spread on the adhesion energies has been reported in the literature (see Ref. 2 and references therein). Similarly, weakening of the adhesion in turbostratic graphite compared with Bernal graphite is expected.[5,116] In a more recent report, Wang *et al.*[99] measured the interlayer shear stress of bilayer graphene by monitoring the strains in the graphene next to the blister but not lifted off the substrate (Figure 2 (e)). Here strain develops as a consequence of sliding. Their data provided evidence of both the lower monolayer sliding on the substrate, and the upper layer sliding on the lower layer. Analysis of the data gave the interfacial shear stress of monolayer graphene on SiO_2 as 1.64 MPa. This was much higher than the interlayer shear stress of bilayer graphene, 40 kPa (1.04 fN/atom). The implication is that the graphene-SiO_2 vdW bonding is much stronger that the weak dispersion vdW bonding that holds the two graphene sheets together.

E. Inelastic X-ray scattering

As discussed in Section III, some key elastic moduli of graphene come directly from the experimental values for graphite, measured by inelastic x-ray scattering (IXS). This measures

the acoustic phonon branches of graphite.[20] The initial slope of these branches along high-symmetry directions gives the sound velocity, and therefore the moduli by Christoffel's equation.[117] IXS is less sensitive to structural defects than ultrasonic methods and it does not have the difficulties in sample size and energy transfer limitations that inelastic neutron scattering suffers.[20] Experimentally IXS employed to measure graphite is not suitable for measurements on graphene due to the small sample volume. The alternative approaches to measure the in-plane elastic moduli of graphene are introduced above, and the results largely depend on interactions of graphene with its surroundings (substrates and/or pressure transmitting media, PTM). Details will be discussed in Section V.

F. Density functional theory

This section particularly addresses properties that are anisotropic in-plane, which have been calculated but not confirmed by experiments. Whereas it is extremely difficult to do any mechanical testing on free-standing graphene, the in-plane graphene mechanical properties calculated by DFT are obtained naturally freestanding, and in vacuum. It is commonly considered that the calculated in-plane elastic constants are accurate (and indeed they are close to the well-established experimental results on graphite)[22] and they are often used to parameterise various empirical models and evaluate the validity of classic simulations.[22,118–121] Strain is the input in a computational model and the resulting energy and stress are calculated. The ease with which the positions of the atoms can be specified enables the investigation of a number of anisotropic in-plane properties that result from strain along specific directions (armchair or zigzag).

The undeformed hexagonal lattice is isotropic. While in-plane uniaxial strain breaks the symmetry, the isotropy remains in the sense that most properties vary with the strain along most directions very similarly, except two specific directions.[122,123] We present clear anisotropic response of four properties to uniaxial strain along zigzag or armchair directions.[121,124,125] Fig. 3 (a) presents that the in-plane Poisson's ratio (corresponding to the elastic modulus c_{12}) shifts differently with uniaxial strain along armchair or zigzag direction, and the stiffness (corresponding to c_{11}) becomes different after 15% strain along armchair or zigzag direction.[124] Fig. 3 (b) shows that stress-strain curves of the shear deformation (relevant to c_{66}) along these two directions are different.[121] The ultimate stress of

graphene along these two directions is also calculated to be different by about 20%.[120] Zhou *et al.* plotted the electron density of graphene at zero, biaxial and uniaxial stress, as shown in Fig. 4.[125] In Fig. 4 (c), the high electron density area (red area) at uniaxial stress along zigzag direction attracts the nuclei at corners more than the central areas of those stretch bonds attracting those corresponding nuclei. That extra attraction stiffens the three-atom bending force constant labeled by k_{angle}, which supports the uniaxial stress. Differently, along uniaxial stress along the armchair direction, the supporting bending force constant (labeled as k_{angle} in Fig. 4 (d)) is stiffened by two high electron density areas (two red areas on the right). This was proposed as a possible interpretation for the anisotropy in ultimate strength[125] and could be relevant to other anisotropic properties.

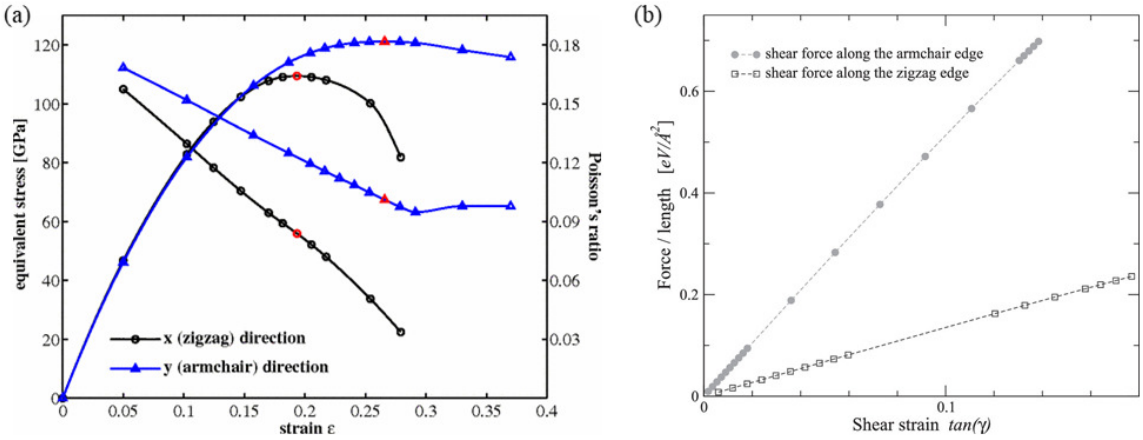

FIG. 3. (a) "The curves connected to the origin are the equivalent tensile stress (d_0=3.34 Å) versus uniaxial strain in the x and y directions, respectively. The lines with initially negative slopes (scale labels to the right) are the finite-deformation Poisson's ratios as functions of the uniaxial strain in the x and y directions, respectively. The red circles and triangles indicate the condition where peak stress could be attained for zigzag and armchair nanotubes, respectively." Reproduced with permission from Phys. Rev. B **76**, 064120 (2007).[124] Copyright (2007) The American Physical Society. (b) "Stress-strain curves for shear deformations of graphene monolayers, obtained through MD simulations. Filled circles (open squares) show results corresponding to shear forces acting on the armchair edge (zigzag edge) of graphene. Dashed lines are guides to the eye." Reproduced from G. Kalosakas, N. N. Lathiotakis, C. Galiotis, and K. Papagelis, Journal of Applied Physics **113**, 134307 (2013),[121] with the permission of AIP Publishing.

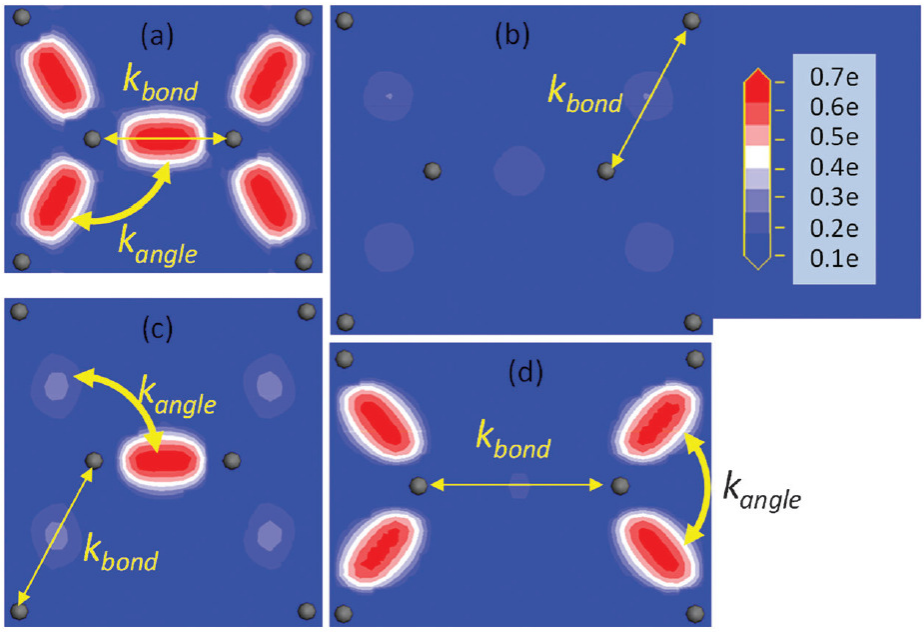

FIG. 4. "The electron density distribution contour of graphene under different tensile loads, (a) ϵ=0; (b) biaxial tension at ϵ=0.28 (the bond stretching ratio ξ= 0.25); (c) uniaxial tension along the zigzag direction at ϵ=0.28 (the bond stretching ratio ξ(Bond I)=0.2, ξ(Bond II)=-0.03); (d) uniaxial tension along the armchair direction at ϵ=0.28 (the bond stretching ratio ξ(Bond I)=0.36, ξ(Bond II)=0.003). Reproduced with permission from Phys. Chem. Chem. Phys. **18**, 1657 (2016).[125] Copyright 2016 The PCCP Owner Societies.

V. GRAPHENE IN INTERACTION WITH ITS ENVIRONMENT AT HIGH PRESSURE

The mechanical properties of graphene can be probed by high pressure. In bulk materials, high-pressure experiments can characterize the bulk modulus and its pressure derivative through the equation of state, which links the volume variation to pressure. Many bulk systems are anisotropic, and have an anisotropic elastic stiffness tensor c_{ij}. With more than one atom per primitive cell, as in graphene, internal strains may occur. Particularly for 2D systems, bond or directional compressibilities can be defined to fully describe the changes in atomic positions due to the deformation under hydrostatic pressure.[126] Graphene is however not only highly anisotropic but also is only one atom thick. While its in-plane deformation modifies the C-C separation or sp^2 bond length, its out-of-plane deformation can only be

described as deformation of the $\pi-$orbitals.

In high-pressure experiments, both the C-C sp^2 bonds and the spatial extension of the $\pi-$orbitals will be modified by interactions with the surrounding PTM (anything from helium, argon, through to water, ethanol or various oils), which itself increases in density with pressure. Interactions between graphene and the surrounding medium can range from weak vdW to strong covalent interactions. In particular, the vdW interactions will become stronger under pressure. The $\pi-$orbitals may become highly modified under pressure, perhaps creating strong dipolar interactions with neighboring molecules. At what point could we consider the system to be something other than graphene (as, *e.g.* graphene oxide)? The effects of pressure may be simply to change the graphene thickness, or may include doping or hybridization. As in any material, the c_{ij} are expected to increase with pressure, but since all the carbon atoms in graphene are in contact with the environment, we may expect that c_{ij} will depend on pressure and temperature, and also on the environment. It is likely that c_{33} will be most influenced by the pressure and the environment. But are the pressure dependencies of other parameters dominated by the pressure or by the environment? How best to compare the pressure responses of graphene and graphite? These issues are addressed here.

Graphene can be studied in suspension, with PTM on both sides, and when the PTM is liquid, the graphene is free of non-hydrostatic strains. When graphene is supported by a substrate, the situation is quite different. We must consider what differences are significant, and what can be learned from these different environments.

This section has three parts treating the pressure response of graphene in the different environments depicted in Fig. 5. First, we will discuss the case of graphene in suspension in a fluid as shown in Fig. 5 (a). Then, the case of supported graphene immersed in a fluid PTM (b). Finally, the case of graphene sandwiched between two different (Fig. 5 (c.1)) or identical (Fig. 5 (c.2)) solids. The Fig. 5 (c) cases are also relevant to help understand the mechanical response of graphene in composite materials.

A. Suspended graphene in a fluid PTM

This may be considered as the paradigmatic pressure experiment, with the two variants of Fig. 5(a). A few Raman scattering experiments have been reported corresponding to

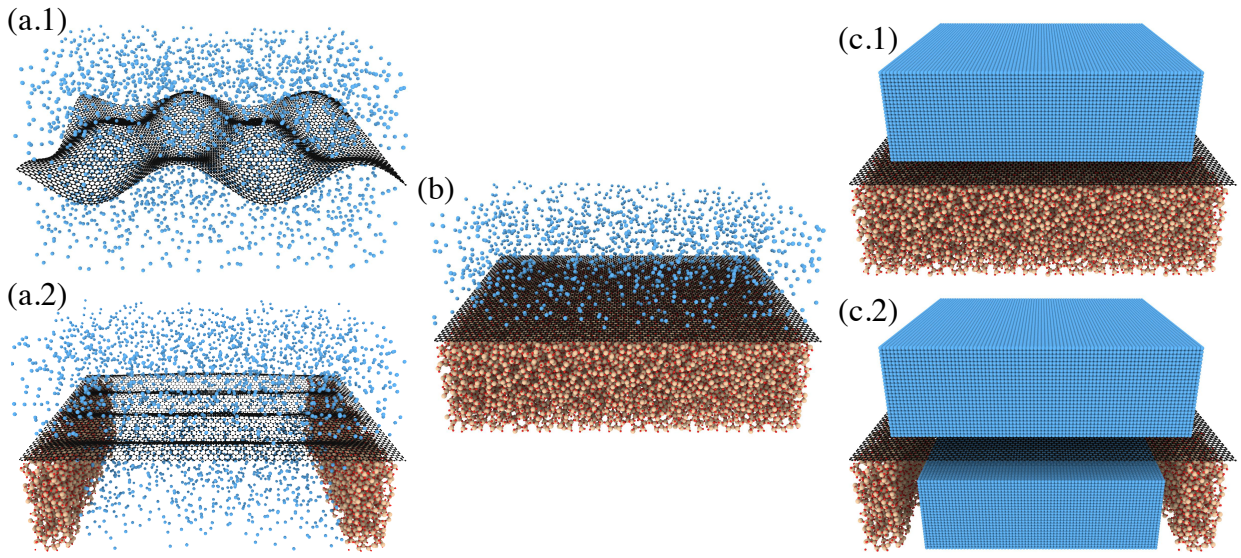

FIG. 5. The various cases encountered in high-pressure experiments and discussed in this section are: (a) suspended graphene in a fluid PTM, (b) supported graphene in a fluid PTM, and (c) graphene sandwiched between two solids. In cases (a) and (c), one needs to distinguish between (a.1) free-standing graphene and (a.2) graphene across a hole ; and (c.1) graphene sandwiched between two different solids and (c.2) graphene in a single solid. The presence of ripples is shown in (a.1) and wrinkles in (a.2).

these configurations: an ensemble of graphene layers in suspension and considered separated each from the others (Fig. 5(a.1)) or supporting an individual graphene layer on a hollowed substrate (Fig. 5(a.2)). In both cases, we may note that the graphene may not be flat due to the spontaneous formation of ripples (Fig. 5(a.1)) and wrinkles (Fig. 5(a.2)).[127,128] Wrinkles and ripples differ by their aspect ratio.[127] Ripples are isotropic, with an amplitude $\sim$ nm, and an aspect ratio ~ 1. Wrinkles are more aligned and larger, having an aspect ratio > 10, due to the partial decoupling of bending and stretching modes.[50,127,128]

In Fig. 5 (a.2), while the graphene sheet may be under tension at ambient pressure (resulting in wrinkles with an axis perpendicular to the trench),[127] we might expect that differential contraction under pressure of the support and the graphene (unless the support is made of diamond) would result in a loss of tension and eventually buckling in a different direction or even crumpling.[127] However, this may be prevented by the evolution of the adhesion of graphene to the internal walls of the trench. Bunch *et al.* observe a minimum

TABLE IV. Summary of high-pressure Raman experiments on suspended graphene.

Type	PTM[1]	$P_{hydrostatic}$ (P_{Max}) [GPa]	$\frac{\partial\omega_G}{\partial P}$ hydro (P_{Max}) [cm^{-1}/GPa]	Ref
suspension[(2)]	N_2	2 (8)	4.7	34
supported[(3)]	Fluorinert	1.0 (4.2)	- (5.6)	37
suspension	DMF	1.6 (7)	5.4	40
supported[(4)]	H_2O	1.0 (35)	- (3.4)	131

(1) see text

(2) The sample were films with a mixture of monolayer, bilayer and few-layer graphene and having 2D characteristic signature of few-layer graphene rather than single-layer graphene.

(3) From the detachment from graphene supported on Si/SiO_2 using as PTM a 1:1 mixture of Fluorinert FC70 and FC77 (nonpolar).

(4) A gold microscopy grid was used to suspend graphene.

non-zero tension,[129] due to this, and analysed by Lu and Dunn.[130]

All high-pressure experiments on suspended graphene have used Raman spectroscopy as a probe. Raman spectroscopy does not give direct access to the pressure evolution of the unit cell parameters which would determine the elastic constants. Raman spectroscopy provides nevertheless a signature of the response of the C-C interatomic potential through the G-mode pressure dependence. Table IV summarizes the most relevant results from suspended graphene studies.

All the studies in Table IV were done using different PTM (FC-70 is perfluorotripentylamine and FC-77 is a perfluorocycloether; DMF is N,N-dimethylformamide). Only two studies (using nitrogen and DMF as the PTM) were performed in hydrostatic conditions throughout the pressure range (*i.e.* with a liquid PTM). On the other hand, the nitrogen PTM study was of a mixture of monolayer, bilayer and few-layer graphene, which makes its results difficult to interpret. The DMF PTM study is the only one in which a G-band pressure dependence has been obtained for a monolayer graphene sample suspended in liquid. This study was able to obtain a $\frac{\partial\omega_G}{\partial P}$ in hydrostatic conditions from a careful analysis from a total of 4 pressure points in the DMF hydrostatic domain up to 1.6 GPa. The value of 5.4 cm^{-1}/GPa was obtained with a linear fit and 5.6 cm^{-1}/GPa with a quadratic fit using

the quadratic coefficient of the graphite fit.[28] These are 15 to 25 % higher than the graphite G-mode slope which is $4.3 - 4.7$ cm^{-1}/GPa using the same quadratic coefficient.[28] This difference is partly due to the non-negligible impact of interlayer-coupling on the in-plane vibrations in graphite (see Sec. VI C). There are reports pointing to PTM-induced charge transfer to graphene in polar media[132,133] even from the first stages of compression,[133] and of pressure-induced reactivity with water.[134] Doping, p or n, leads to an enhanced value of the G-mode frequency[135] which may explain an increase of the G-mode pressure coefficient in graphene. Experiments using an inert PTM would clarify whether there is a difference between graphene in-plane elastic constants and those of graphite, or if the observed differences are related to polarization-induced modifications of the electronic structure of graphene.

Another interesting aspect is that, as pressure is increased, the PTM fluid viscosity increases. The vdW graphene-fluid interaction may overcome the thermal energy of the fluid molecules. An organized fluid layer may then appear in contact with graphene. This constitutes a loss of 2D character which may also affect the mechanical properties of graphene and may explain differences in the Raman response with different PTM. DFT and MD modelling - DFT is performed at zero temperature - have in fact shown in carbon nanotubes under high pressure the formation of a structurally coherent contact layer of CO_2 or water around carbon nanotubes.[136,137] In fact, DFT modelling shows that in carbon aromatic systems such as benzene, vdW interaction plays an important role in phase stability at high pressures.[138]

We may conclude this part by underlining that dipole or other enhanced VdW interactions with the PTM molecules and the possible loss of 2D character through the formation of a PTM contact layer need to be explored as possible mechanisms modifying the graphene mechanical properties at high pressure.

B. Supported Graphene in a fluid PTM

This is the case depicted in Fig. 5 (b), *i.e.* graphene on a substrate and immersed in a fluid PTM. In this case, the PTM applies hydrostatic pressure on the graphene-substrate system. With increasing pressure, the substrate (unless it is diamond) contracts much faster than the graphene, which puts the graphene under a large biaxial compression. How much graphene contracts and is strained in response to the substrate shrinking is governed by the

graphene-substrate adhesion and friction, graphene/PTM adhesion, graphene stiffness, and graphene bending modulus. We will now discuss the role of each parameter.

1. *Role of the substrate*

Graphene stiffness is one of the largest-ever measured, with a Young's modulus of ~ 1 TPa (Table II),[25,139] while its bending stiffness is often considered as negligible;[140,141] indeed so small that it is hard to measure in a direct manner. Many reported values (depending on the temperature and flake size) are often about 1 eV,[142] and it was measured in carbon nanotubes as 1.7 eV (see Sec. III D 5).[45] Thus, it is expected that graphene will tend to bend or wrinkle rather easily in order to relieve in-plane compression.[143–145] The interaction between the graphene layer and its supporting surface, namely the graphene-substrate adhesion, is therefore an extremely important parameter governing the graphene response to biaxial compression: if the graphene-substrate adhesion is poor, the graphene will not fully follow the substrate's deformation and instead will slide or wrinkle to reduce its stress. However, the adhesion of graphene to its substrate is an intricate mixture of (a) the interaction energy between carbon and surface atoms, (b) substrate surface roughness, (c) graphene number of layers, (d) commensurability of the graphene and substrate lattices, and (e) the normal force from the PTM, which must modify the effects of (a) to (d). As a consequence, each graphene-substrate system is unique and the amount of strain transferred from the substrate to the graphene layer can only be assessed in a phenomenological way, for example with a "strain transfer efficiency" parameter α.[38,146] Now to discuss each of these parameters:

(a) The strength of the graphene-substrate interaction energy can be assessed from the graphene-substrate distance, which varies greatly from one substrate type to another – as shown in Table I which gives some experimentally measured distances. Graphene deposited on metals tends to form covalent bonds that greatly decrease the graphene-substrate distance. This would correspond to a much increased adhesion energy and forces for peeling off and for sliding. One thus expect the strain transfer efficiency α to be close to 1 in such systems – and $\alpha = 1$ for a copper substrate was indeed observed up to a critical stress of 2 GPa.[34,38] Moreover, the history of the graphene sample plays a huge role in the interaction with its substrate: whether the graphene was transferred or grown on the substrate has a large impact on its adhesion and residual stress. As discussed in Sec. III D 3, epitaxial

graphene is under large strain after cooling (hence showing $\alpha = 1$), whereas CVD (usually on Cu) graphene shows the occurrence of ripples to release the stress (resulting in a $\alpha < 1$). An even lower α on Cu is expected if graphene is transferred onto it.

(b) When the surface roughness is too high, total unbinding from the substrate surface can occur, at ambient pressure[145,147] or under high pressure.[37] Some substrates show the occurrence of a critical stress beyond which the strain transfer efficiency is greatly diminished,[38] which is probably due to a partial unbinding of the graphene layer from its substrate. While not measured experimentally, this critical stress is supposed to be roughness-dependent for a given substrate. The substrate surface roughness also greatly influences the *friction* between the graphene layer and its substrate, which in turns plays a role on the mechanism of the mechanical response of graphene to biaxial compression. When the strain transfer efficiency $\alpha < 1$, it means that either (a) graphene slips all over the substrate; or (b) graphene wrinkles, ripples or crumples. Or a combination of (a) and (b) may occur. In the case of a rough substrate with a conforming graphene (as is the case most of the time), case (a) has an extended energy cost because it involves the whole graphene surface, while case (b) only involves the local elastic energy cost of buckling. Depending on the substrate roughness, a varying proportion of slipping and buckling may thus occur. However, the application of a normal force by the hydrostatic pressure to the surface will certainly hinder the formation of wrinkles or ripples. Wrinkles were however observed under hydrostatic pressure (at 4 GPa) even in nano-graphite ($\sim$ 30-layer graphene).[148]

(c) In the same manner, adhesion to a rough substrate is decreased when the number of graphene layers increases, *i.e.* when the graphene bending rigidity increases.[36] With an increasing number of layers, the conformation of graphene to its rough substrate may decrease, resulting in a decreased friction. We may note that in MoS_2, which has a much higher bending stiffness than graphene, a bimodal behavior has been seen when supported on Si/SiO_2. A mixture of regions showing strong adhesion and other regions showing weak adhesion was seen.[149]

(d) Finally, it was for example shown that for a given substrate such as Co(0001), the graphene-substrate distance decreases when the graphene lattice is matched with the substrate lattice,[150] allowing for covalent C-Co bonding. Such an effect therefore plays a large role on the starting *stress+doping* state of graphene. In the following however, we will not consider substrates in which this type of interaction may happen. Pressure-induced doping

effects will then be due essentially to interaction with the PTM and will be discussed in the following subsection. One should also note that the (in)commensurability of the lattices should also play a role in the friction between graphene and its substrate.

(e) All these parameters may be impacted by the modification of the graphene-substrate distance due to the application of pressure. However, in pressure ranges for which the PTM is liquid (hydrostatic pressure), the graphene Raman response is always linear,[34,37,38,40,131,133] which tends to show that this effect is limited at pressures below $\sim$ 10 GPa.

The mechanical response of graphene to high pressures is usually followed through *in situ* Raman spectroscopy, as stress induces a deformation of the carbon bonds and thus shifts the Raman features such as the G-mode (ω_G) or the 2D-mode (ω_{2D}). But similar shifts can also arise from doping. Graphene is a π-conjugated 2D material, thus its electronic structure is highly sensitive to its environment. This charge sensitivity allows doping through gating or intercalating ("substrate doping", see *e.g.* Ref. 151 for a review), but it can also occur due to the interaction with polar molecules in the PTM which can be enhanced at high pressure[133] ("PTM doping"). Overall, the doping and strain contribution to the ω_G shift can be unravelled by following the slope of $\partial\omega_{2D}/\partial\omega_G$[151,152] (see Fig. 6). Finally, the substrate type and the graphene preparation method (as-prepared, transferred, synthesised, exfoliated...) play a large role in the ω_G frequency[150,151] and the graphene-substrate distance (Table I). Large variations of the ω_G peak position can be observed for graphene on a substrate according to the crystallographic orientation, matching or random. For example, while ω_G = 1581 cm^{-1} for free graphene, it redshifts down to 1452 cm^{-1} for oriented graphene on Co(0001), and it can vary between $\sim$1550 and 1600 cm^{-1} across a single sample of misaligned graphene on Co(0001).[150] In the case of Co(0001), matching the graphene and substrate lattice orientations allows chemical bonding between the two, resulting in a shortening of the graphene-substrate distance and a significant stretching of the graphene lattice, thus decreasing the ω_G frequency. However, this is peculiar to Co(0001) as, usually, the CVD synthesis of graphene on a metallic substrate results in a compressive stress of the graphene layer, and thus an increased ω_G frequency.[151] On the other hand, the incommensurability of both lattices can result in large local variations of the ω_G position, that can be due to both strain and/or doping.

In conclusion, the substrate plays a very important role both at ambient pressure and under high pressure. Before the application of pressure, and together with the history of

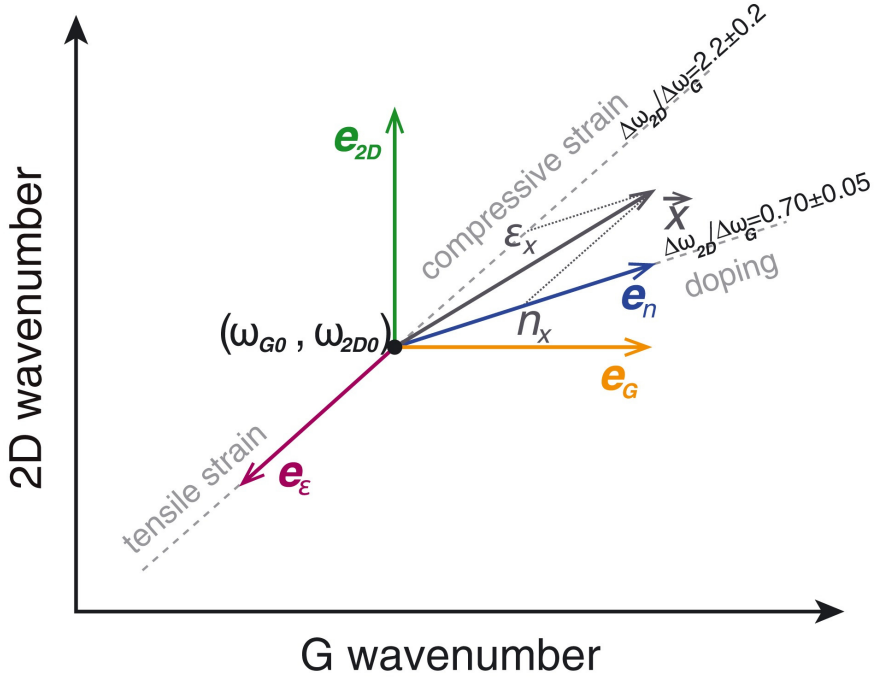

FIG. 6. Lee diagram[152] allowing retrieving the strain and doping (ε_X and n_X) at a point X in the (ω_G, ω_{2D}) space. The origin $(\omega_G, \omega_{2D})_0$ is the reference state at ambient conditions. Reproduced with permission from J. Raman Spectrosc. **49**, 130 (2018).[151] Copyright 2018 John Wiley & Sons, Ltd.

the sample, the substrate determines the reference state of the graphene, *i.e.* the graphene-substrate distance as well as the initial stress and doping states. During pressure application, it determines the strain of the graphene layer through the phenomenological parameter α, this strain being relative to the initial state. It is inappropriate to consider the evolution of the Raman G-mode frequency as a function of pressure;[38] rather, it should be considered as a function of the strain, the actual strain depending on the reduction of the substrate dimensions. Overall, in the simple case where $\alpha = 1$ and *in the absence of doping*, a Raman G-mode frequency dependence on substrate strain ε of $\frac{\partial \Delta\omega_G}{\partial \varepsilon} = -60 \pm 3\ \mathrm{cm}^{-1}/\%$ is expected.[38] Since $\frac{\omega}{\omega_0} = (1+\varepsilon)^{-2\gamma_{E_{2g}}}$ for in-plane biaxial compression,[34] this corresponds to a Grüneisen parameter $1.8 < \gamma_{E_{2g}} < 2.0$ – in excellent agreement with uniaxial strain experiments[33] and *ab initio* modeling.[153] This further confirms the importance of substrate-induced biaxial strain on the properties of graphene.

2. *Role of the PTM*

a. Mechanical response When the PTM is fluid, it has a much larger compressibility than the substrate. This, of course, is of no importance while it exerts purely hydrostatic pressure. However, fluid PTM display large viscosities at pressures in the GPa range, and local crystallisation of the fluids occurs at the graphene surface.[154] Whatever the state of the PTM, this configuration results in a biaxial stress field in the system: the top surface of the graphene layer is in contact with the fluid that applies hydrostatic stress, while its bottom surface is in contact with the solid substrate which imposes a bi-axial stress that is determined by the equation of state of the substrate. By symmetry, there are no shear stresses σ_{xz} and σ_{yz} applied to the graphene, except at the edges and other lateral inhomogenities.

In the case of monolayer graphene, the mechanical response of the graphene layer is mainly governed by the substrate.[34,36–38,146] In the case of bilayer graphene, that remains so while the PTM remains liquid[133] (however, after solidification of the PTM, a stress gradient between layers could be measured, as will be discussed in the next section). One might expect, indeed, that the application of pressure would result in an increased graphene-substrate adhesion by reducing the graphene-substrate distance; and also that it would prevent the graphene layer from buckling and hence forming wrinkles or ripples. As mentioned in (b) above, substrate surface roughness can cause a critical stress above which the graphene layer is not able to follow the deformation of its substrate.[38] So the reality is more complex: despite gigapascals of pressure applied on the graphene layer, it seems that it is still able to buckle to reduce stress.[148]

To sum up, while the PTM remains liquid, the evidence is that the *mechanical response* of graphene is fully governed by the adhesion to the substrate. This goes for mono- and bilayer graphene only; for thicker samples the graphene bending rigidity increases and the adhesion to the (usually rough) substrate is reduced, leading to a mechanical response closer to graphite.[36,146]

b. Electronic response Comparing inert PTM (such as Ar, N_2) with polar PTM (such as 4:1 methanol:ethanol), a significant increase in the pressure coefficient of the Raman G-band was reported, from ~ 7 to ~ 10 cm^{-1} GPa^{-1} for SiO_2/Si substrate), for both mono- and bilayer graphene.[36] This change was however later refuted.[37,38] Nevertheless, a pressure-

induced decrease of the G-band FWHM was observed when using 4:1 methanol:ethanol PTM, which was attributed to a doping contribution.[36] However, it was not clear whether this doping remained constant over the whole pressure range.[37] A recent study of twisted isotopically-labelled bilayer graphene in 4:1 methanol:ethanol PTM by Forestier *et al.*[133] clarified the doping effect of the PTM. Here, the observation of a difference in the response of the two layers made it possible to conclude that there was a pressure-induced doping due to the alcohol PTM: the G-mode of the upper layer in contact with the PTM showed a larger pressure shift than the lower layer in contact with the substrate, demonstrating the occurrence of a doping due to the polar PTM which increases with pressure. It is worth mentioning here that the isotopically-labelled bilayer graphene of this study is made of two CVD graphene layers transferred on top of each other, resulting in a sample behaving like two independent layers on top of each other. The difference in isotopic masses decouples the G-modes of the two layers, so that they can be separately resolved.

C. Graphene sandwiched between two solids

The investigation of the mechanical behavior of graphene monolayers and bilayers interacting with solids under pressure on both sides, as in Fig. 5 (c), constitutes an interesting route to better understand the mechanical properties of graphene-based nanocomposites.

Under sufficient pressure, any fluid transforms to a solid at ambient temperature. Therefore, increasing the pressure sufficiently in the two situations discussed in the previous subsections, the systems will evolve to i) graphene between two different solids (Fig. 5 (c.2), for supported graphene on a substrate) or ii) graphene between two identical solids (Fig. 5 (c.1), for graphene in suspension). This leads to an asymmetrical or to a symmetrical environment.

Crystallization of the PTM has at least two effects. First, macroscopically, it modifies the stress field with the appearance of differential strain at the graphene-PTM interface. Second, microscopically, it creates a periodic potential in interaction with the graphene sheet.

1. Different solids

Crystallization of the PTM when compressing a supported graphene leads to an asymmetry of the environments and of the associated stress fields. Each side of the graphene plane

is in contact with a different solid medium. However, the change of state (fluid to solid) of the PTM is usually unnoticed in high-pressure Raman spectroscopy on supported monolayer graphene.[146] The preferred PTM are soft vdW solids (such as argon or nitrogen) and are considered to provide quasi-hydrostatic conditions even after solidification.[155] The bonding of such solids only leads to weak vdW type interactions with the graphene. The interactions between these solids and the graphene can only marginally modify the pressure-induced behavior which remains dominated by the effect of the substrate.[146]

In contrast, crystallization of the PTM is clearly observed by Raman spectroscopy experiments on bilayer graphene where each layer experiences different conditions. The signature of the solidification is a change in the pressure-dependence of the G-peak position and/or a change of the width of this peak. The change of slope may be attributed to additional differential strain components and the broadening is related to inhomogeneity of the stress field. As the spectroscopic signatures are mainly affected by these external effects, it is difficult to assess any intrinsic effect, *i.e.* any modification of the elastic properties of graphene.

The difference of the applied stress on each side of a twisted bilayer graphene have been evidenced and quantified by the high-pressure Raman experiment on isotopically labelled bilayer graphene mentioned in Sec. V B 2 b. Strain differences up to $\sim 0.1\,\%$ between the two graphene layers were observed when applying pressures of up to 10 GPa with nonpolar solid environments.[133]

2. Identical solids

There are only a few reports of high-pressure experiments on graphene in suspension above the crystallization pressure of the PTM. It represents a major experimental challenge to characterize and manipulate a mono- or bi-layer, to load it in a high-pressure cell as suspended and to follow experimentally the high-pressure behavior across and above the solidification of the PTM. A particularly important issue is the form of suspension. If the graphene is freely floating in the PTM, then after solidification it will be subject to the strain of the PTM as pressure is further increased and the sample volume decreases and changes shape. However, if the graphene is supported over a trench in a substrate, then after solidification it will be pressed down into the trench, as the PTM will typically be much more compressible than the substrate, and this will put the graphene under high

tensile strain.

Table IV includes data from studies before and after solidification of the PTM. Sun *et al.* dissolved PMMA on which CVD-grown graphene had been transferred.[40] The solvent (DMF) was used as the PTM. So this graphene was assumed to be freely-floating. The G-peak pressure coefficient changed at around 2 GPa, from 5.4 cm^{-1}/GPa to 7.5 cm^{-1}/GPa. This was interpreted as resulting from the adhesion to the more compressible solid PTM, with the strain transmission effect as for supported graphene. In Tao *et al.*[131] bilayer graphene suspended on Au grid was sandwiched between ice in different phases. It was not possible to fit the G-band data evolution using the quadratic term of graphite determined by Hanfland *et al.*[28] Tao *et al.* report a linear G-band evolution with a low pressure coefficient of 3.4 cm^{-1}/GPa up to pressures of 40 GPa[131] without any noticeable variation at the PTM freezing point. Filintoglou *et al.* [37] observed graphene sandwiched in solid fluorinert and obtained a G-band pressure slope of 5.4 cm^{-1}/GPa. These results, with G-band pressure coefficients between 3.4 and 7.5 cm^{-1}/GPa, show the extreme sensitivity of graphene to the nature of the PTM, and the details of the experiment influencing the transmitted strain. Solidification has a drastic impact for suspended graphene, contrary to the previous case, supported graphene, for which the solidification has almost no noticeable effect. The high-pressure mechanical response of graphene can be related to graphene composites. In particular, and not surprisingly, it has been shown that the level of adhesion between graphene and polymer matrix is a key factor in the mechanical response of nanocomposites.[156,157]

After solidification (crystallization or vitrification), the main issue the nature of the applied stress that includes shear components. However, one may consider the effect of the increasing pressure on the intrinsic mechanical properties of graphene, especially the c_{33} elastic constant. Increasing interaction between π-orbitals and the surrounding solid media can strongly modify the π-orbitals and hence perhaps the sp^2 bonds.A detailed quantification will be introduced in Sec. VI C. This seems to be especially true of polar PTM that exhibit piezo-doping and ultimately the formation of covalent bonds.[134] In this case, graphene cannot be considered still as an isolated system under external perturbation.

VI. DRESSED GRAPHENE

A. Functionalisation

Graphene can react with, for instance, oxygen, hydrogen or fluorine. When covalent bonds develop with other molecules in low proportions we may speak about defective graphene. When those bonds develop extensively we will prefer to speak about other materials, some aperiodic, such as graphene oxide, some periodic, such as graphane (hydrogenated graphene monolayer) or diamane (hydrogenated bilayer of graphene)[158] (see Fig. 7) or fluorinated single-layer diamond.[159] In these cases there will be either local or extended modifications of the covalent graphene bonding scheme, with a modification of the associated elastic stiffness constants. For single-layer graphene oxide, the experimental Young's modulus derived from AFM measurements is substantially reduced to 207.6 ± 23.4 GPa.[160] As most of these other materials are new, their properties are derived from *ab initio* calculations.[161] For instance it has been shown by DFT calculations that graphene oxide with increasing proportions of (-O) or (-OH) displays a progressive elongation of the C-C bond and a softening of the mechanical properties.[162]

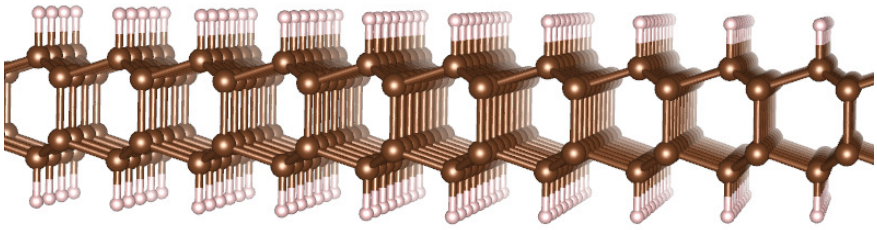

FIG. 7. Diamane structure with sp^3 bonding for C atoms.

B. Derivative geometry

We may also consider making a nanotube by rolling up a graphene sheet until we connect the edges through covalent bonds. This change in geometry leads to a topologically different graphene-based system, the carbon nanotube. Of course, the synthesis of carbon nanotubes does not correspond with this *gedanken* experiment, which, rather, raises the issue whether carbon nanotubes should be considered to be a material, derived from graphene by the

change in geometry, or to be a structure made of graphene. Many DFT calculations find that the in-plane Young's modulus of small-diameter carbon nanotubes walls is reduced, due to the curvature-induced modification of the C-C hybridization. We may then expect that extensively corrugated, ripple or wrinkled graphene could exhibit an average bonding scheme differing from flat graphene and hence with different local 2D elastic stiffness constants as well as the large-scale reduced stiffness due to the corrugation. See Sec. VII for further discussion of nanotubes.

C. Effect of vdW interactions

Geometry and covalent bonding have an effect on the 2D elastic stiffness constants of graphene. What about vdW interactions? Consider the difference between graphene in graphite and in epitaxially grown bilayer graphene, two different cases of vdW graphene stacking. In graphite the vdW distance between graphene layers is 3.35 Å which may be considered as the graphene thickness in that particular case (see Sec. II A and Table I). In bilayer graphene grown on a SiC(0001) surface, the measured graphene-graphene distance is 3.24 Å.[163] In multilayer graphene grown on an SiC substrate, the distance between graphene layers is found to be 3.9 Å after the first graphene layer in contact with the SiC substrate.[164] X-ray diffraction measurements have revealed a certain degree of rotational disorder in the stacking of these graphene layers.[116] Do these differences in thickness imply changes in the C-C sp2 bonding?

The thickness of graphene in these different cases is to be related to the extension of its π-orbitals. This is certainly a point of view in rupture with the Galilean continuum mechanics approach, but wholly consistent with the modern approach to the radius of atoms. In vacuum, of course, quantum mechanics tells us that the spatial extension of the π-orbitals electron cloud is to infinity, like the hydrogen 1s state. Any definition of a finite extension of an electron orbital in vacuum (such as the Bohr radius) is thus entirely arbitrary. Indeed such definitions are better described as characteristic lengths (such as the Bohr radius) which are not arbitrary, but also not obviously the extension or size of the atom. Where the pi-orbitals of a graphene monolayer are delimited by meeting the electronic orbitals of adjacent materials, their extension is to be defined in just the same way as the size of atoms is defined (see Sec. II A and V).) In the case of graphite, it is very simple - the distance to the point

between the graphene layers about which the π-electron density is symmetrical. In the case of a graphene monolayer with other materials either side, or multilayer graphene in other than Bernal stacking, we need to seek criteria (as with the size of atoms in multi-element mixtures and compounds) which allow the consistent attribution of a thickness to, e.g. the side of a graphene monolayer in contact with another layer in AA or in turbostratic contact, and also to the other side in contact with perhaps sapphire. We should certainly define the graphene thickness in the asymmetric context as the addition of two different contributions on each side of the carbon nuclei.

Practically, the shift of the G-mode frequency under out-of-plane compression is a suitable quantity to quantify the weak modification of the in-plane elastic constants by deformation of π-orbitals. The G-mode, as mentioned previously, is an in-plane anti-phase vibration of C-C atom pairs and is therefore closely related to the in-plane stiffness of graphene and graphite. Its eigenvectors (E_{2g}) in graphene and graphite are shown in Fig. 8. The dynamical equation of a 1D spring can be written as $Ku = \omega^2 u$, where K is the force constant, u is the displacement and ω is the frequency. And it can be extended to 2D for the G-mode of graphene:[166]

$$\begin{pmatrix} \omega_0^2 & 0 \\ 0 & \omega_0^2 \end{pmatrix} \begin{pmatrix} u1 \\ u2 \end{pmatrix} = \omega^2 \begin{pmatrix} u1 \\ u2 \end{pmatrix}, \tag{11}$$

where the u_1 and u_2 are the relative displacement of the two carbon atoms along the two equivalent in-plane directions, as the hexagonal lattice of graphene is isotropic in-plane. When an additional graphene layer is added, Eq. 11 becomes[167]

$$\begin{pmatrix} \omega_0^2 & 0 & C & 0 \\ 0 & \omega_0^2 & 0 & C \\ C & 0 & \omega_0^2 & 0 \\ 0 & C & 0 & \omega_0^2 \end{pmatrix} \begin{pmatrix} u1 \\ u2 \\ u3 \\ u4 \end{pmatrix} = \omega^2 \begin{pmatrix} u1 \\ u2 \\ u3 \\ u4 \end{pmatrix}, \tag{12}$$

where u_3 and u_4 are the displacement of the two carbon atoms in the added layer, and C accounts for the interlayer coupling. The longitudinal and transverse modes are not coupled due to the hexagonal lattice, hence all the zero elements in the force constant tensor. The solutions to the secular equation of Eq. 12 are

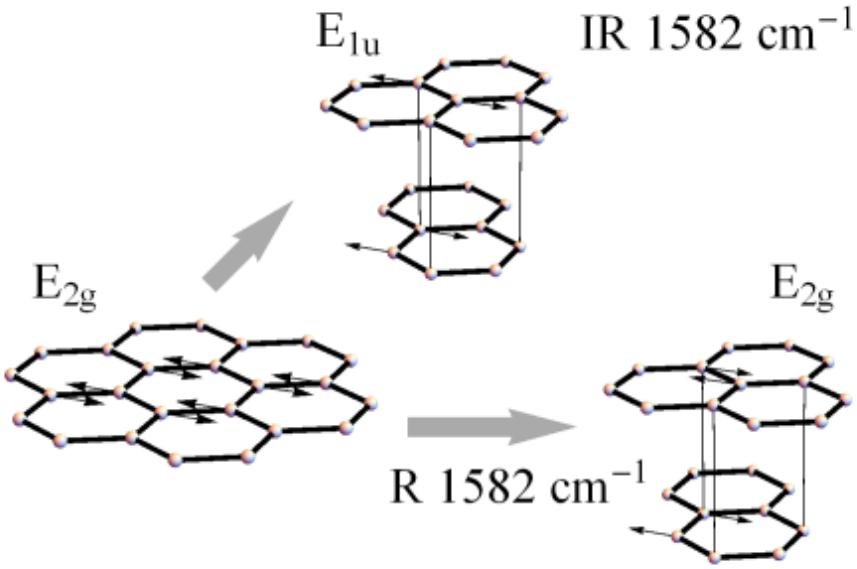

FIG. 8. "Phonon eigenvectors of graphene and graphite. Every phonon eigenvector of graphene gives rise to two vibrations of graphite. For example, the in-phase combination of the two layers for the E_{2g} optical mode of graphene yields $E_{2g} \otimes A_{1g} = E_{2g}$ and the out-of-phase combination $E_{2g} \otimes B_{1u} = E_{1u}$. Next to the graphite modes it is indicated whether they are Raman (R) or infrared (IR) active and the experimentally observed phonon frequencies. The translations of graphite are omitted from the figure." Reproduced with permission from Phil. Trans. Roy. Soc. A **362**, 2271 (2004).[165] Copyright 2004 The Royal Society.

$$\omega^2_{(1)} = \omega_0^2 + C$$
$$\omega^2_{(2)} = \omega_0^2 + C$$
$$\omega^2_{(3)} = \omega_0^2 - C$$
$$\omega^2_{(4)} = \omega_0^2 - C$$

The two different solutions correspond to the E_{1u} and E_{2g} G-modes of graphite, where carbon atoms in both layers in a unit cell vibrate in-plane and in anti-phase, but the vibrations of the two layers are in-phase and out-of-phase, respectively. Typical experimentally measured values of the graphite E_{1u} and E_{2g} frequencies are 1587 and 1580 cm^{-1}, respectively.[27,168] From the measured frequencies of E_{1u} and E_{2g} of graphite, we can calculate the ω_0=1583.5

cm^{-1} for the G-mode of a graphene plane in graphite – the G-mode frequency of graphene should be slightly higher than graphite, even their in-plane stiffnesses are the same.

To quantify the effect of deformation of the π-orbitals on the G-mode frequency, we can introduce out-of-plane strain and calculate the shift of G-mode frequency. The off-diagonal term C in Eq. 12 for interlayer coupling can be expanded in terms of out-of-plane strain ε_{zz}. The diagonal terms can be expanded too, to account for the possible modification of the in-plane sp^2 bond stiffness by the compression of the π-orbitals,

$$\begin{pmatrix} \omega_0^2 + A\varepsilon_{zz} & 0 & C + B\varepsilon_{zz} & 0 \\ 0 & \omega_0^2 + A\varepsilon_{zz} & 0 & C + B\varepsilon_{zz} \\ C + B\varepsilon_{zz} & 0 & \omega_0^2 + A\varepsilon_{zz} & 0 \\ 0 & C + B\varepsilon_{zz} & 0 & \omega_0^2 + A\varepsilon_{zz} \end{pmatrix} \begin{pmatrix} u1 \\ u2 \\ u3 \\ u4 \end{pmatrix} = \omega^2 \begin{pmatrix} u1 \\ u2 \\ u3 \\ u4 \end{pmatrix} \tag{13}$$

and the solution to the secular equation is:

$$\begin{aligned} \omega_{(1)}^2 &= \omega_0^2(E_{2g}^{(2)}) + (A + B) \times \varepsilon_{zz} \\ \omega_{(2)}^2 &= \omega_0^2(E_{2g}^{(2)}) + (A + B) \times \varepsilon_{zz} \\ \omega_{(3)}^2 &= \omega_0^2(E_{1u}) + (A - B) \times \varepsilon_{zz} \\ \omega_{(4)}^2 &= \omega_0^2(E_{1u}) + (A - B) \times \varepsilon_{zz} \end{aligned}$$

which indicates an increasing E_{1u} and E_{2g} splitting , and therefore different shift rates with pressure of these two modes. Without the contribution from the coupling to adjacent layers, the G-mode frequency of graphene under out-of-plane compression is $\omega = \omega_0 + A \times \varepsilon_{zz}$. Sun *et al.* calculated the G-mode frequencies of graphite under out-of-plane compression by DFT, and introduced a new parameter γ' to compare the contribution from out-of-plane strain on with that from in-plane strain:[167]

$$\frac{\Delta\omega}{\omega_0} = -\gamma(\varepsilon_{xx} + \varepsilon_{yy}) \mp \frac{1}{2} SDP(\varepsilon_{xx} - \varepsilon_{yy}) - \gamma'\varepsilon_{zz} \tag{14}$$

where γ is the Grüuneisen parameter and SDP is the shear deformation potential. The values of γ' are -0.0131 and 0.0585 for E_{2g} (GM) and E_{1u} of graphite, respectively, and the value for the GM of graphene is in the middle. These values, compared to a typical value 1.90 of the Grüuneisen parameter for the in-plane strain contribution,[33,62,166] are indeed very small. However, both graphene and graphite are about 30 times more compressible out-of-plane than in-plane.[20] So, under hydrostatic compression, the contribution to the G-mode

frequency from out-of-plane compression, while smaller than the in-plane contribution, is not negligible.

Three useful points can be summarised from the above discussion: first, deformation of π-orbitals can modify the in-plane bond stiffness by a non-negligible amount, especially when the vdW interaction between graphene and the surrounding medium increases under compression; second, although the G-mode is a good measure of in-plane stiffness, its frequencies in graphene and graphite are slightly different even if the in-plane stiffnesses are the same; and third, the shift rate of the monolayer graphene G-mode with pressure should be higher than that graphite, because for the graphene G-mode, there is no impact from the coupled vibration in adjacent layers.

Returning to the issue of different vdW interaactions with different media at ambient pressure, some authors have proposed that the graphene layers in multilayer graphene on 4H-SiC(0001) behave as monolayer graphene[116] due to the predominant rotational stacking faults weakening the graphene-graphene interaction. Hence, following the same principle of thickness definition, the flat turbostratic (free-standing) graphene thickness will be 3.9 Å, *i.e.* $\sim$6.5 % greater than the vdW graphite distance.

We may then conclude that different schemes of vdW stacking lead to changes in the π-orbitals. If we need to consider effects on the 2D elastic stiffness constants of the π-orbitals, then they should be considered as affected by graphene stacking schemes. The effect of such changes on the sp^2 bonds are from deformed π-orbitals modifying the in-plane C-C sp^2 bonds. The weak modifications of the C-C sp^2 bonds by the π-orbitals can be quantified in detail as above. In particular, as graphene is little affected by weak van der Waals interactions or geometry variations with curvatures less than about ~ 1 nm^{-1}, the electronic structure bonding scheme determining the 2D elastic constants of graphene is preserved. Flat or weakly bent graphene in vacuum or in graphite or in single-wall and multi-wall nanotubes may be then considered as having the same 2D elastic constants as graphite.

VII. CARBON NANOTUBES: PROPERTIES OF GRAPHENE

Carbon nanotubes, particularly single-walled and double-walled carbon nanotubes, are interesting structures in their own right (but that is outside the scope of this review). They

provide perhaps the only way in which graphene can be studied free-standing and in vacuum - graphene with nothing touching either side and nothing to constrain it in-plane either. Closed nanotubes provide the opportunity to study graphene with vacuum inside and other media outside, while open-ended nanotubes provide other possibilities. Most important, and our focus here, they can reveal aspects of the mechanical properties of graphene, such as its bending stiffness, that are difficult or impossible to study in other forms of graphene. Many of the opportunities to learn about graphene by studying nanotubes have not yet been fully exploited, as we shall see below.

Most of the work we discuss depends on Raman spectroscopy, observing the G-mode and the other graphene/graphite phonons, but crucially the radial breathing mode (RBM) which has no equivalent in graphite.

A. G-mode in nanotubes

The G-mode has the inconvenience that it is hard to resolve the contributions of nanotubes of different diameters and chiralities. For that reason, much more attention has been paid to the RBM (Sec. VII B).

The G-mode frequency is sensitive to confinement effects, dynamical effects, and curvature, which lift the degeneracy to give G^+ and G^- peaks.[169] In Piscanec *et al*,[169] the effect of curvature is deduced from the difference between experimental phonon wavenumbers and calculations and obeys $\Delta\omega = -\zeta \times d^{-2}$. Values are given for the TO mode (circumferential motion) with $\zeta = 25.16$ cm^{-1}·nm^2 and LO modes (axial motion) with $\zeta = 12.0$ cm^{-1}·nm^2. Up to now, there is no direct calculation of the curvature effect. However, it can be estimated from a simple continuum model. We consider the thickness of the graphene h_G and treat the electrons on both sides (i for inner and o for outer) in a first approximation as a continuous medium. The tension (o) and compression (i) are opposite but not equal, giving a strain at the centre. Energy equilibrium gives $\epsilon_i^2 \times (d/2 - h_G/4) = \epsilon_o^2 \times (d/2 + h_G/4)$. For a curved plate, we have: $\epsilon_o = h_G/2d$. So we deduce the average strain for the center to be $< \epsilon >= (\epsilon_i + \epsilon_o)/2 = h_G^2/(8d^2)$. Using the strain coefficient -57 cm^{-1}/% ,[170] we find $\Delta\omega_{TO} = -80.0 \times d^{-2}$. This gives the correct dependence on d but too large a value for ζ. However, a homogenous medium is not a satisfactory model for graphene (*c.f.* the Yacobson paradox, Sec. II A). Refining the model as a structure, (σ bonds at the centre, and π for

the inner and outer material), the relation is the same but the coefficient is different. From energy equilibrium, we have $\epsilon_\sigma = \sqrt{\frac{c_{11}^\sigma(h_G-h_\sigma)}{c_{11}^\pi h_\sigma}} \times \epsilon_\pi = \sqrt{\frac{c_{11}^\sigma(h_G-h_\sigma)}{c_{11}^\pi h_\sigma}} \times \epsilon_\pi = 0.170 \times \epsilon_\pi$ leading to $\Delta\omega_{TO} = -13.6 \times d^{-2}$, which is in a more reasonable range and $\epsilon_\sigma = \frac{2.38\times10^{-3}}{d^2}$, to be compared with $\frac{1.6\times10^{-3}}{d^2}$ from calculation.[171]

B. RBM in nanotubes

In the RBM fundamental, all atoms move radially together. The restoring force is straightforwardly due to c_{11}, and the frequency depends inversely on the diameter, and to a much lesser extent on the chirality, in the 100-300 cm^{-1} region of the spectrum. Moreover, tunable excitation picks out those tubes that are resonant with the excitation wavelength. Consequently, very detailed studies of the RBM have been reported.[172]

Simple models can account for this mode using continuous mechanics or atomic descriptions. We start by supposing the nanotube wall to consist of a 2D sheet of continuum material with the 2D graphene elastic constants $c_{11}^{2D} = c_{11}d = 372$ Nm^{-1} and $c_{12}^{2D} = c_{12}d = 47$ Nm^{-1} . In the RBM motion, the wall has tangential strain but no axial strain (the RBM frequency is too high to induce any axial motion), so the relevant elastic stiffness constant is c_{11}^{2D}. In contrast, the approach of Mahan,[173] modelling with a three-dimensional isotropic plate, invokes not only c_{11} but also c_{12}, which is incorrect. The potential energy per unit length of tube at the extreme of a sinusoidal motion $r = A\cos\omega t$ is

$$U_{max} = \frac{1}{2}c_{11}^{2D}\epsilon^2 \times 2\pi R_C = \pi R_C c_{11}^{2D}\frac{A^2}{R_C^2} \tag{15}$$

while the kinetic energy at the center of the motion is

$$E_{max} = \frac{1}{2}mA^2\omega^2 = \frac{1}{2}A^2\omega^2 \times 2\pi R_C N m_0 \tag{16}$$

where $N = 3.8 \times 10^{19}$ is the number of carbon atoms of mass m_0 in a unit area of graphene. Equating U_{max} and E_{max}, and rearranging, we have

$$\omega_{RBM} = \frac{1}{R_C}\sqrt{\frac{k_{11}}{Nm_0}} \equiv \frac{235}{d(nm)}\text{cm}^{-1} \tag{17}$$

where the diameter $d = 2R_C$, in excellent agreement with experiments.[174] At much higher frequency, 1590 cm^{-1}, the G-mode phonon corresponds to atomic motion in antiphase. To

relate the RBM to the G-mode considering atomic motion, a 1D model (atoms equispaced around a circle) has been proposed by Gerber *et al.*[175] leading to :

$$\omega_{RBM} = \frac{a_0}{d}\omega_G = \frac{0.142\text{nm} \times 1590\text{cm}^{-1}}{d(\text{nm})} = \frac{226}{d(\text{nm})}\text{cm}^{-1} \tag{18}$$

in excellent agreement with Eq. 17. Considering a 2D system, the equations are the same because the E_{2g} G-mode is doubly degenerate in the plane allowing the basis to be aligned with the chiral vector, which is the circumference. The approximation here is that the G-mode degeneracy is not lifted by the curvature.

For nanotubes in a medium (e.g. a liquid or nanotube bundles) the vdW interaction leads to an upshift of the RBM frequencies above the values of Eq. 17 by some $10 - 20$ cm^{-1}. The stiffening of the vdW interaction under pressure is largely responsible for the further increase of RBM frequencies under pressure.[136]

The phonon spectrum of nanotubes includes also the soft modes, in the $10 - 100$ cm^{-1} spectral region, which are the higher-order modes of a series in which the RBM is the zeroth member. Unlike the RBM, the soft modes depend on the bending stiffness D. The n^{th} soft mode has $2n + 2$ nodes around the circumference of the tube. They should soften under pressure, and would go to zero frequency at the collapse pressure. However, like the RBM, they are raised in frequency by the vdW interaction with the PTM, and the increase in this interaction with pressure actually results in the soft modes stiffening instead of softening under pressure.[176]

C. SWCNTs under pressure

The pressure dependence of single-walled nanotubes provides two opportunities at least to learn about graphene. The diameters of nanotubes are usually given as defined by the nuclear positions, in contrast to taking the outside diameter over the electron orbitals. That is what the general formula $d = a_0\sqrt{n^2 + mn + m^2}$ gives, and that is the diameter usually considered when analysing the response of nanotubes to high pressure, for example, the rate of shift of the G-mode and RBM phonon frequencies under pressure. If the pressure P were applied at the radius $r = d/2$, pressure coefficients of, for example, the G-mode phonon would be expected to be approximately r/h times the graphite or graphene pressure coefficients, where h is the relevant graphene thickness (see Sec. II A). (A full analysis would take into

account the differing tangential and axial stresses in a tube under pressure, respectively Pr and $Pr/2$.) However, if the graphene has a thickness h and the pressure is applied at a radius $r + h/2$, the stresses on the sp^2 bonds will be greater and the pressure coefficients correspondingly increased. How much they are increased, however, depends critically on the mechanical properties of graphene and their response to pressure and bending. We are not aware of a full analysis along these lines of the nanotube pressure coefficients. The situation is further confused by the stiffening of the RBM mode which is largely due to the increasing vdW interaction between the PTM and the nanotube,[136] and also by any effects of the PTM on the graphene as discussed in the previous section, which may account for the different pressure coefficients reported for nanotubes in different PTM.[177–180]

D. SWCNT Collapse

At sufficiently high pressures or large diameters, nanotubes collapse. Collapse of nanotubes under high pressure has also been challenging, not least because, apparently as obvious a case of Euler buckling as the collapse of pillars, the collapse of tubes under external hydrostatic pressure is mathematically intractable. Many experimental observations have been interpreted as corresponding to collapse, at a very wide range of pressures, and fitted to a variety of theoretical equations. A complete solution for the simple (ideal) elastic ring was reported only in 2011.[181] Good agreement with the Levy-Carrier formula for a thin-walled tube, $P_C = \frac{3D}{R^3}$ where D is the bending stiffness was confirmed, and the collapse to a peanut shape above P_C was found to be quite slow, complete only at about $1.5P_C$.[182] Torres-Dias *et al.* reported that this fitted experimental data for the quenching of the RBM for a range of SWCNT diameters, giving an estimate of $D = 1.7$ eV.[45]

Some caveats must be mentioned. First, the effects of the thickness h need to be known and taken into account, as for the pressure coefficients. Also, it is clear that vdW interactions will reduce the collapse pressure, so that SWCNTs tubes above about 4 nm will spontaneously collapse (the same physics as the folding of Sec. III D 6). This scarcely affects smaller tubes where the bending energies involved are very much greater. Then, for diameters below about 1 nm, Torres-Dias *et al.*[45] reported that the collapse pressure is reduced below the Levy-Carrier formula. This is quite a strong effect, observed experimentally and in theoretical modelling,[45] and also previously noticed by Elliott *et al.*[183] It extrapolates to

$P_C = 0$ for a diameter of about 0.4 nm, not much smaller than the smallest nanotubes ever reported.[184] One source of this behaviour could be softening of the bending potential with angle. Another source is the reduction in the Euler buckling load even of straight pillars when the compliance is discretised rather than continuous. This effect is reported by Carter et al,[77] and discussed in Sec. III D 5. Both of these explanations remain to be analysed in detail.

When the diameter of a SWCNTs is large enough, *i.e.* above about 5 nm, a spontaneous collapse occurs. This leads to a cross-section in the form of a dogbone or peanut with a twist along the axis[185] if the SWCNT is free (in liquid or gas for example). The cavities of the edges have a diameter of the order of C_{60} fullerene, like the cavities of folded graphene (Section III D 6) while the stacking depends on the chirality.[186] Indeed, the phenomenonis very closely related to folding, with the same balance between adhesion energy and bending stiffness. Like folding, it has not been fully exploited to refine our knowledge of these two important mechanical parameters of graphene.

Del Grande *et al.*[187] note that the energy barrier for a circular tube to collapse is many eV, so it should not be possible for it to happen through thermal activation – but once initiated at one point in the tube, the collapse will readily propagate along the tube. This is not an uncommon situation in condensed matter physics. It may be compared with the initiation of plastic deformation in a perfect crystal, where the activation energy for the creation of a dislocation is very high, or with boiling in a pure liquid, where the activation barrier for the formation of a bubble is very high. In these examples as in doubtless many others, it is a local defect, impurity, or perturbation that breaks the impasse. Del Grande *et al.* suggest that the collapse of large SWCNTs is likely to be produced by small mechanical stresses that naturally occur during synthesis. The nanoscale force required to initiate collapse, to bypass the energy barrier, is about 5 nN[187] which is easily achievable in AFM compression experiments.[188]

E. DWCNTs coefficients under pressure

While the mechanical behaviour of SWCNTs under pressure is reasonably well understood as described in the previous section, double-walled nanotubes provide further opportunities - and challenges - to better understand the mechanical properties of graphene. Again, these

opportunities come from the pressure coefficients of the phonon modes while the tubes remain circular, and then from the collapse pressures and modes of collapse. Many papers report pressure coefficients of the Raman G-modes of the outer and inner walls of DWCNTs which are not dissimilar. Yet it is hard to understand how the external pressure may be transmitted to the inner tube, given the enormous anisotropy of the graphite elastic stiffness tensor. Moreover, the sum of the reported pressure coefficients of the inner and outer tube is usually considerably in excess of the coefficient of an empty outer tube, *i.e.* an SWCNT of the same diameter. Yet the load on the walls of the inner and out tubes should sum to the load of an SNCNT of the same diameter, and so therefore should the pressure coeficients.

Experimentally, pressure transmitted to an inner nanotube can be monitored by the upshift of the GM or RBM. The former should be less dependent on the PTM as the upshift is from the C-C bond stiffening under pressure, whereas the latter is from the increasing interaction of a tube with its surroundings. Consequently, it is easier to describe the GM pressure coefficient. The experimental challenge to monitor pressure by the GM frequency is the assignment of the GM to tubes of a specific diameter and chirality, and, further, to distinguish inner and outer tubes in DWCNTs. While the RBM is diameter-dependent, tubes of different diameters have very similar GM frequency, if not the same, at ambient condition. An ideal situation would be to have only one RBM and its corresponding G-mode dominating the spectrum (either due to a special sample containing only one chirality, or having only one chirality in resonance at a specific laser excitation). Many factors can add to the complication of the situation: 1) common CNT samples contain tubes of many different chiralities; 2) many more than one chirality can be in resonance or close to the resonance condition; 3) while the outgoing laser energy is only shifted by 10 – 20 meV for the RBM, the difference is 200 meV for the GM, making it possible that the GM is in resonance with the outgoing laser while its corresponding RBM is far from the resonance condition; 4) for DWCNTs, one has to further assign Raman peaks to the outer or the inner tube, and the interaction between inner and outer tubes modifies the Kataura plot,[172]. In particular, Hirschmann *et al.*[189] showed that the wall-to-wall distance between inner and outer tubes in DWCNTs increases with increasing tube diameters, which makes the RBM upshifts of the inner tubes from intertube interaction no longer a constant, as most earlier work supposed. This requires further caution on the assignment of RBMs to inner tubes, but can be used to refine our calculations if needed.

Early studies on DWCNTs under pressure observed at least two components in a GM profile, shifting with pressure at different rates. It is tempting to assign these two components to outer and inner tubes for two reasons, one is that stress transmitted to the inner tube should be lower than hydrostatic pressure, resulting in two different responses to pressure, and the other is that outer (or inner) tubes in resonance at the same condition can have very close diameters and they should response similarly to pressure. Among various work, the GM pressure coefficients can be different, as different tubes are in resonance; they can be either PTM dependent, as PTM modifies the transition energy of CNTs, making different tubes in resonance, or PTM independent as no other charility in those samples is available near the resonance condition. The results of these high pressure study on DWCNTs are summarised in Table V below.

TABLE V. Experimental shift rates of DWCNTs GM with pressure.

Outer tube ($cm^{-1}GPa^{-1}$)	Inner tube ($cm^{-1}GPa^{-1}$)	PTM	Laser Excitation (nm)	Reference and notes
9.6	6.4	paraffin oil	514	Ref. 190
8.4	5.5	NaCl	514	Ref. 190
5.8	3.3	methanol-ethanol	633	Ref. 191
6.9	4.1	Oxygen	633	Ref. 191
8.6	5.1	Argon	633	Ref. 191
5.5	4.3	methanol-ethanol	514	Ref. 192

In this section we have seen that much could be learned about the mechanical properties of graphene from further experimental and theoretical work on nanotubes, particularly under pressure. The major obstacle is that the RBM modes are highly resonant and the resonances shift with pressure. For the G-mode, this means that as pressure increases, different diameter tubes (which are not well-resolved) may dominate the Raman spectrum at different pressures.[193] For the RBM the tubes of different diameters and chiralities are well-resolved. However, both for identifying or for choosing which tubes are observed, and for tracking given tubes over a substantial pressure range, tunable Raman excitation is needed (*e.g.* a dye laser or Ti-sapphire laser), together with a tunable Raman spectrometer. The number of laboratories worldwide with such equipment, and also a high-pressure capability,

is small indeed.

VIII. MODELS FOR THE MECHANICS OF GRAPHENE

Mechanical properties, more perhaps than any other properties of matter, invite the construction of models, for purposes ranging from visualisation, through understanding, to prediction. We comment briefly here on what can be suitably expressed by or learnt from different models, starting from the simplest. Continuum models for graphene have been considered. The flat plate of isotropic material and a thickness chosen to give the right bending stiffness was mentioned in Section II A. While useful for considering the behavious of graphene as a beam, plate or shell, the model does not attempt to replicate the thickness a_{33} or the out-of-plane compressibility c_{33} of graphite. For that reason a continuum model was considered in which the nuclei and the sp^2 bonding orbitals were treated as an infinitely thin sheet with the 2D c_{11} and c_{12} values of graphene, sandwiched between two layers of soft material modelling the pi-orbitals.[39] This model could replicate the thickness, the bending stiffness and the out-of-plane compressibility by a suitable choice of an anisotropic 3D elastic tensor for this soft material. The model is suitable for considering the behaviour of, for example, nanotubes under pressure (see above, Sec. VII C). For example, it can be used to consider questions such as the radius at which a nanotube is loaded by external pressure. It is also a model that can be readily discretised as a ball-and-spring model. In this case, the nuclei are the balls, the sp^2 bonds are springs (2D stretching potentials) between them and the pi-orbitals are springs that terminate on a point that is not an atom. These points could also be joined by springs that give the bending stiffness.[39] That introduces the question, whether this is the physically-realistic representation of the origin of the bending stiffness of graphene, or whether it actually arises from the torsional stiffness of the sp^2 bonds through 4-atom potentials in-plane. A comparison with the torsional vibrational modes of ethane (sp^3) and ethylene (sp^2) could be useful here,

At this point we are approaching the valence force field (VFF, Keating) models[194] and those used in MD and Monte Carlo simulation. Keating, however, used only two-atom (stretch) and three-atom (angular) springs, or interactions, with nearest neighbours only to model the elastic constants c_{ij} and internal strains of, *e.g.* silicon. Keating did not consider phonon frequencies. It is in considering the phonons as well as the elastic constants that

Keating models tend to break down.

In MD simulation, Ref. 26 used two-atom interactions with atoms out to the fifth-nearest neighbours to model the phonon frequencies and the phonon dispersions. The necessity to include the fifth-nearest neighbours is demonstrated by investigating the origin of the GM frequency. Consideration of the 2D bulk modulus, or area modulus A, gives the force constant of the C-C bonds as 748 N/m, or 46.7 eV/A^2, from the experimental values of elastic constants of graphite.[20]. We assume that the GM frequency comes only from the nearest C-C stretching, and we can obtain the GM frequency as 1450 cm^{-1}. The gap to the experimental value of about 1580 cm^{-1} can be filled by other contributions beyond the nearest neighbour. Quantifying these contributions requires more information than the frequency of LO at Γ point (G-Mode)[27] in the phonon dispersion relation of graphite. We have already given an example that one has to include the second nearest neighbour out-of-plane interaction to describe the separation of E_{1u} and E_{2g}. It was found that up to the fourth nearest neighbour interaction has to be included to well fit the dispersion from Γ point to M (especially the initial increase of E_{1u} frequency from Γ point),[41] obtained by inelastic neutron scattering.[42]. A further fifth nearest neighbour interaction was included to fit more recent in-elastic x-ray data, which gave a finer description of the local minimum of TO at K point.[26] Surprisingly, the empirical force constant model including up to the fifth nearest neighbour that fits well the experimental data of the full phonon dispersion of graphite (as shown in Fig. 9), gives a force constant for the nearest neighbour C-C stretching, as small as 25.88 eV/A^2, indicating that about half of the contributions to the C-C vibrational frequency in graphite come from other interactions than the nearest C-C stretching. This is truly unexpected, yet explaining the existing data best.

Despite contributing only half to the G-mode frequency, the nearest C-C stretching is expected to contribute dominantly to the upshift of G-mode with pressure from Pauli exclusion, which is a measure of C-C bond anharmonicity. The evolution of the phonon dispersion relation in graphite would not only verify or dispute the small value of the nearest C-C force constant, but also quantify the anharmonicity, when it becomes available. We should point out that in addition to in-plane contributions, the GM frequency can also be modified by deformed π-orbitals from out-of-plane, as discussed in section VI B.

It is clear that Keating potentials are not generally capable of representing both the elastic constants and the phonon frequencies, and certainly fail in this regard for graphene.

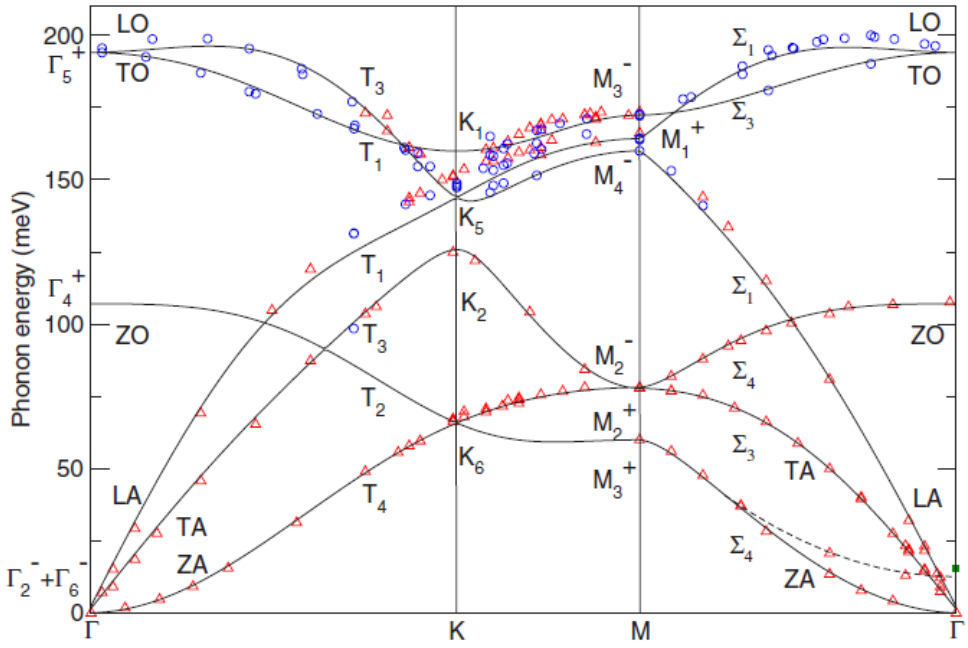

FIG. 9. Phonon dispersion of graphite from inelastic x-ray scattering (symbols). Triangles are from Ref. 26. Circles are from Ref. 195. Squares are INS data from Ref. 42. Solid lines are the fit of experimental data by a force constant model including up to the fifth-nearest neighbor. The dashed line is a quadratic extrapolation of the data. Reproduced with permission from Phys. Rev. B **76**, 035439 (2007).[26] Copyright (2007) The American Physical Society.

It is not clear from the literature what the simplest models are that can do this, nor if such a model is physically interpretable (two-atom interactions between fifth-nearest neighbours do not have any obvious physical interpretation). On the other hand, VFF models continue to be developed and exploited for various purposes, *e.g.* thermomechanical properties[196] and phonon frequencies.[197]

Usually, molecular dynamics modelling uses optimized reactive potentials (multi-body potentials such as the second generation reactive empirical bond order (REBO) potential of Brenner[198] or the recent implementation of the ReaxFF potential[199]) which allow the study of mechanical properties at the nanoscale such as fracture. An example is the finding that fracture requires a force of about 8 nN per C=C bond.[200] This is equivalent to about 90 GPa uniaxial stress and compares with the 130 GPa strength reported by Lee *et al.*[25] in AFM nanoindentation (see also Fig. 3 (a)).

Turning to quantum-mechanical models, the simple tight-binding description is used for

obtaining the electronic structure[201] but is not suitable for mechanical properties.

DFT provides models that can be made to replicate experimental data excellently.[22] However, apart from the maps of electron density, there is little in DFT output that can assist a physical understanding of the predicted properties. It could be said that in graphene research as in high-pressure research, the greatest value of DFT is that it can tell us what happens under experimental conditions that are not (yet) accessible to experimenters. For that reason we discuss it under different headings above. An example in graphite is the determination of c_{13} (Sec. III A, see also Sec. IV F).

IX. CONCLUSIONS

This paper reviews the mechanical properties of graphene, both those that are expected to be similar to graphite and those expected to be different from graphite – and anomalies. Graphene is commonly called a 2D material, which implies a thickness tending to zero. However, the π-electrons above and below the 2D plane of carbon nuclei extend the electron density of monolayer graphene into the third dimension, perpendicular to the 2D plane. For example, we can define a vdW thickness of graphene, 3.35 Å, which is the experimentally measured spacing of graphene layers in graphite. One key conclusion is that, far from being a 2D material, graphene has a well-defined 3D structure, which may be modelled in various ways to help understand its mechanical properties. That is not to say that it cannot display 2D physics, much as can a 100 Å quantum well – which has a 3D physical structure of *e.g.* GaAs sandwiched between GaAlAs. Following from that, those of its mechanical properties which are related to those of graphite are indeed very similar, if not identical.

Without neighboring layers, unsupported graphene is not mechanically stable and has intrinsic ripples. The low bending stiffness further promotes the formation of ripples, making them common in graphene samples. It also contributes to the softening of the ZA phonon dispersion, resulting in a negative thermal expansion (although, again, it is not clear whether this is significantly different from that of graphite). Properties such as the out-of-plane stiffness, though expected to be similar to graphite, require indirect approaches to define and to quantify.

Due to the small sample size of exfoliated graphene – at least out-of-plane – experiments to measure many of its mechanical properties requires special design. In addition, the

environment surrounding graphene adds further complexity to the interpretation of these experimental data, from determining factors as substrates transferring strain to graphene, to subtle modification by influencing the π-orbital distribution.

There are many derivative structures from graphene, in a way making the extraordinary properties of graphene tunable. They can also be used to help understand the properties of graphene. Among those, measurements on carbon nanotubes in some circumstances give the most accurate values for mechanical properties of graphene, perhaps even better than measurements on graphene itself, as nanotubes can be self-supporting, free-standing, and stable, thus excluding many of those complexities.

Finally, composite materials in which matrix material is reinforced mechanically by the inclusion of graphene flakes are perhaps one of the most exciting applications in which the mechanical properties of graphene are central. Many other so-called 2D materials are also used, and their mechanical properties are often less well characterised than those of graphite. One may expect them to be related to the corresponding bulk materials much as graphene is related to graphite.

ACKNOWLEDGMENTS

DGP acknowledges the support from "Graphene Core 3" GA: 881603 which is implemented under the EU-Horizon 2020 Research and Innovation Actions (RIA) and is financially supported by EC-financed parts of the Graphene Flagship.

DATA AVAILABILITY

Data sharing is not applicable to this article as no new data were created or analyzed in this review.

REFERENCES

[1]D. G. Papageorgiou, I. A. Kinloch, and R. J. Young, Progress in Materials Science **90**, 75 (2017).

[2]D. Akinwande, C. J. Brennan, J. S. Bunch, P. Egberts, J. R. Felts, H. Gao, R. Huang, J.-S. Kim, T. Li, Y. Li, K. M. Liechti, N. Lu, H. S. Park, E. J. Reed, P. Wang, B. I.

Yakobson, T. Zhang, Y.-W. Zhang, Y. Zhou, and Y. Zhu, Extreme Mechanics Letters **13**, 42 (2017).

[3]B. Sundqvist, Physics Reports (2021), https://doi.org/10.1016/j.physrep.2020.12.007.

[4]G. Galilei, *Dialogues Concerning Two New Sciences by Galileo Galilei* (New York: Macmillan, New York, 1914).

[5]M. Short and P. Walker Jr, Carbon **1**, 3 (1963).

[6]B. I. Yakobson, C. J. Brabec, and J. Bernholc, Phys. Rev. Lett. **76**, 2511 (1996).

[7]W. L. B. M.A, The London, Edinburgh, and Dublin Philosophical Magazine and Journal of Science **40**, 169 (1920).

[8]W. P. Davey, Phys. Rev. **19**, 248 (1922).

[9]R. W. G. Wyckoff, Proc Natl Acad Sci U S A **9**, 33 (1923).

[10]G. W. Stewart, Phys. Rev. **33**, 889 (1929).

[11]A. Camerman and J. Trotter, Acta Cryst **18**, 636 (1965).

[12]F. Jean, T. Zhou, N. Blanc, R. Felici, J. Coraux, and G. Renaud, Phys. Rev. B **91**, 245424 (2015).

[13]P. Sutter, J. T. Sadowski, and E. Sutter, Phys. Rev. B **80**, 245411 (2009).

[14]I. Razado-Colambo, J. Avila, D. Vignaud, S. Godey, X. Wallart, D. P. Woodruff, and M. C. Asensio, Sci. Rep. **8**, 10190 (2018).

[15]X. Fei, L. Zhang, W. Xiao, H. Chen, Y. Que, L. Liu, K. Yang, S. Du, and H.-J. Gao, J. Phys. Chem. C **119**, 9839 (2015).

[16]D. Eom, D. Prezzi, K. T. Rim, H. Zhou, M. Lefenfeld, S. Xiao, C. Nuckolls, M. S. Hybertsen, T. F. Heinz, and G. W. Flynn, Nano Lett. **9**, 2844 (2009).

[17]A. Dahal and M. Batzill, Nanoscale **6**, 2548 (2014).

[18]Y. Gamo, A. Nagashima, M. Wakabayashi, M. Terai, and C. Oshima, Surface Science **374**, 61 (1997).

[19]G. E. Bacon, Acta Cryst **4**, 558 (1951).

[20]A. Bosak, M. Krisch, M. Mohr, J. Maultzsch, and C. Thomsen, Phys. Rev. B **75**, 153408 (2007).

[21]O. L. Blakslee, D. G. Proctor, E. J. Seldin, G. B. Spence, and T. Weng, Journal of Applied Physics **41**, 3373 (1970).

[22]N. Mounet and N. Marzari, Phys. Rev. B **71**, 205214 (2005).

[23]M. Birowska, K. Milowska, and J. Majewski, Acta Phys. Pol. A **120**, 845 (2011).

[24]A. G. Kolpakov, Journal of Applied Mathematics and Mechanics **49**, 739 (1985).

[25]C. Lee, X. Wei, J. W. Kysar, and J. Hone, Science **321**, 385 (2008).

[26]M. Mohr, J. Maultzsch, E. Dobardžić, S. Reich, I. Milošević, M. Damnjanović, A. Bosak, M. Krisch, and C. Thomsen, Phys. Rev. B **76**, 035439 (2007).

[27]F. Tuinstra and J. L. Koenig, The Journal of Chemical Physics **53**, 1126 (1970).

[28]M. Hanfland, H. Beister, and K. Syassen, Phys Rev B **39**, 12598 (1989).

[29]L. Zhenxian, W. Lizhong, Z. Yongnian, C. Qilang, and Z. Guangtian, J Phys Cond Mat **2**, 8083 (1990).

[30]M. Peña-Álvarez, E. del Corro, V. G. Baonza, and M. Taravillo, J Phys Chem C **118**, 25132 (2014).

[31]F. Ding, H. Ji, Y. Chen, A. Herklotz, K. Dörr, Y. Mei, A. Rastelli, and O. G. Schmidt, Nano Lett **10**, 3453 (2010).

[32]M. S. Dresselhaus, A. Jorio, M. Hofmann, G. Dresselhaus, and R. Saito, Nano Letters **10**, 751 (2010).

[33]T. M. G. Mohiuddin, A. Lombardo, R. R. Nair, A. Bonetti, G. Savini, R. Jalil, N. Bonini, D. M. Basko, C. Galiotis, N. Marzari, K. S. Novoselov, A. K. Geim, and A. C. Ferrari, Phys Rev B **79**, 205433 (2009).

[34]J. E. Proctor, E. Gregoryanz, K. S. Novoselov, M. Lotya, J. N. Coleman, and M. P. Halsall, Phys Rev B **80**, 073408 (2009).

[35]Y. W. Sun, D. Holec, D. Gehringer, O. Fenwick, D. J. Dunstan, and C. J. Humphreys, Phys. Rev. B **101**, 125421 (2020).

[36]J. Nicolle, D. Machon, P. Poncharal, O. Pierre-Louis, and A. San-Miguel, Nano Lett **11**, 3564 (2011).

[37]K. Filintoglou, N. Papadopoulos, J. Arvanitidis, D. Christofilos, O. Frank, M. Kalbac, J. Parthenios, G. Kalosakas, C. Galiotis, and K. Papagelis, Phys Rev B **88**, 045418 (2013).

[38]C. Bousige, F. Balima, D. Machon, G. S. Pinheiro, A. Torres-Dias, J. Nicolle, D. Kalita, N. Bendiab, L. Marty, V. Bouchiat, G. Montagnac, A. Gomes de Souza Filho, P. Poncharal, and A. San-Miguel, Nano Lett **17**, 21 (2017).

[39]Y. W. Sun, D. J. Dunstan, M. A. Hartmann, and D. Holec, PAMM **13**, 7 (2013).

[40]Y. Sun, W. Liu, I. Hernandez, J. Gonzalez, F. Rodriguez, D. Dunstan, and C. Humphreys, Physical Review Letters **123**, 135501 (2019).

[41]R. Al-Jishi and G. Dresselhaus, Phys. Rev. B **26**, 4514 (1982).

[42]R. Nicklow, N. Wakabayashi, and H. G. Smith, Phys. Rev. B **5**, 4951 (1972).

[43]R. Saito, G. Dresselhaus, and M. Dresselhaus, *Physical Properties of Carbon Nanotubes* (Imperial College Press, 1998).

[44]S. Siebentritt, R. Pues, K.-H. Rieder, and A. M. Shikin, Phys. Rev. B **55**, 7927 (1997).

[45]A. C. Torres-Dias, T. F. Cerqueira, W. Cui, M. A. Marques, S. Botti, D. Machon, M. A. Hartmann, Y. Sun, D. J. Dunstan, and A. San-Miguel, Carbon **123**, 145 (2017).

[46]A. H. Castro Neto, F. Guinea, N. M. R. Peres, K. S. Novoselov, and A. K. Geim, Reviews of Modern Physics **81**, 109 (2009).

[47]A. K. Geim and K. S. Novoselov, Nature Materials **6**, 183 (2007).

[48]L. Shi, P. Rohringer, M. Wanko, A. Rubio, S. Waßerroth, S. Reich, S. Cambré, W. Wenseleers, P. Ayala, and T. Pichler, Phys. Rev. Materials **1**, 075601 (2017).

[49]Y. Hernandez, V. Nicolosi, M. Lotya, F. M. Blighe, Z. Sun, S. De, I. McGovern, B. Holland, M. Byrne, Y. K. Gun'Ko, J. J. Boland, P. Niraj, G. Duesberg, S. Krishnamurthy, R. Goodhue, J. Hutchison, V. Scardaci, A. C. Ferrari, and J. N. Coleman, Nature Nanotechnology **3**, 563 (2008).

[50]A. Fasolino, J. H. Los, and M. I. Katsnelson, Nat. Mater. **6**, 858 (2007).

[51]J. C. Meyer, A. K. Geim, M. I. Katsnelson, K. S. Novoselov, D. Obergfell, S. Roth, C. Girit, and A. Zettl, Solid State Communications Exploring graphene, **143**, 101 (2007).

[52]R. Zan, C. Muryn, U. Bangert, P. Mattocks, P. Wincott, D. Vaughan, X. Li, L. Colombo, R. S. Ruoff, B. Hamilton, and K. S. Novoselov, Nanoscale **4**, 3065 (2012).

[53]O. M. Marago, F. Bonaccorso, R. Saija, G. Privitera, P. G. Gucciardi, G. Iati, Maria A.and Calogero, P. H. Jones, F. Borghese, P. Denti, V. Nicolosi, and A. C. Ferrari, ACS Nano **4**, 7515 (2010).

[54]P. Thibado, P. Kumar, S. Singh, M. Ruiz-Garcia, A. Lasanta, and L. Bonilla, Physical Review E **102**, 042101 (2020).

[55]J. M. Carlsson, Nature Materials **6**, 801 (2007).

[56]J. E. Proctor, D. M. Armada, and A. Vijayaraghavan, *An Introduction to Graphene and Carbon Nanotubes* (CRC Press, 2017).

[57]P. R. Shaina, L. George, V. Yadav, and M. Jaiswal, J. Phys.: Condens. Matter **28**, 085301 (2016).

[58]F. Jean, T. Zhou, N. Blanc, R. Felici, J. Coraux, and G. Renaud, Phys. Rev. B **88**, 165406 (2013).

[59]H. Pierson, *Handbook of Carbon, Graphite, Diamond and Fullerenes: Properties, Processing and Applications* (Noyes Publications, 1993).

[60]A. Bailey and B. Yates, Journal of Applied Physics **41**, 5088 (1970).

[61]B. Marsden, A. Mummery, and P. Mummery, Proc. R. Soc. A. **474**, 20180075 (2018).

[62]Z. H. Ni, W. Chen, X. F. Fan, J. L. Kuo, T. Yu, A. T. S. Wee, and Z. X. Shen, Phys. Rev. B **77**, 115416 (2008).

[63]M. Senn, A. Bombardi, C. Murray, C. Vecchini, A. Scherillo, X. Luo, and S. Cheong, Phys. Rev. Lett. **114**, 035701 (2015).

[64]W. Miller, C. W. Smith, D. S. Mackenzie, and K. E. Evans, J Mater Sci **44**, 5441 (2009).

[65]M. T. Dove and H. Fang, Rep. Prog. Phys. **79**, 066503 (2016).

[66]L. Wang, Q. Zheng, J. Z. Liu, and Q. Jiang, Phys. Rev. Lett. **95**, 105501 (2005).

[67]Y. Huang, J. Wu, and K. C. Hwang, Phys. Rev. B **74**, 245413 (2006).

[68]O. A. Shenderova, V. V. Zhirnov, and D. W. Brenner, Critical Reviews in Solid State and Materials Sciences **27**, 227 (2002).

[69]M. A. Hartmann, M. Todt, F. G. Rammerstorfer, F. D. Fischer, and O. Paris, EPL **103**, 68004 (2013).

[70]M. M. J. Treacy, T. W. Ebbesen, and J. M. Gibson, Nature **381**, 678 (1996).

[71]D.-B. Zhang, E. Akatyeva, and T. Dumitrică, Phys. Rev. Lett. **106**, 255503 (2011).

[72]J. Peng, J. Wu, K. C. Hwang, J. Song, and Y. Huang, Journal of the Mechanics and Physics of Solids **56**, 2213 (2008).

[73]D. Sen, K. S. Novoselov, P. M. Reis, and M. J. Buehler, Small **6**, 1108 (2010).

[74]A. Politano, A. R. Marino, D. Campi, D. Farías, R. Miranda, and G. Chiarello, Carbon **50**, 4903 (2012).

[75]M. K. Blees, A. W. Barnard, P. A. Rose, S. P. Roberts, K. L. McGill, P. Y. Huang, A. R. Ruyack, J. W. Kevek, B. Kobrin, D. A. Muller, *et al.*, Nature **524**, 204 (2015).

[76]N. Lindahl, D. Midtvedt, J. Svensson, O. A. Nerushev, N. Lindvall, A. Isacsson, and E. E. B. Campbell, Nano Lett. **12**, 3526 (2012).

[77]D. Carter, D. Dunstan, W. Just, O. Bandtlow, and A. S. Miguel, (2020), arXiv:2011.14120 [cond-mat.other].

[78]C. Zhang, K. Bets, S. S. Lee, Z. Sun, F. Mirri, V. L. Colvin, B. I. Yakobson, J. M. Tour, and R. H. Hauge, ACS Nano **6**, 6023 (2012).

[79]A. Impellizzeri, P. Briddon, and C. Ewels, Physical Review B **100**, 115410 (2019).

[80]J. Zhang, J. Xiao, X. Meng, C. Monroe, Y. Huang, and J.-M. Zuo, Physical Review Letters **104**, 166805 (2010).

[81]Z. Liu, K. Suenaga, P. J. Harris, and S. Iijima, Physical Review Letters **102**, 015501 (2009).

[82]S. Cranford, D. Sen, and M. J. Buehler, Applied Physics Letters **95**, 123121 (2009).

[83]X. Chen, C. Yi, and C. Ke, Applied Physics Letters **106**, 101907 (2015).

[84]D.-B. Zhang, E. Akatyeva, and T. Dumitrică, Physical Review Letters **106**, 255503 (2011).

[85]P. H. Tan, W. P. Han, W. J. Zhao, Z. H. Wu, K. Chang, H. Wang, Y. F. Wang, N. Bonini, N. Marzari, N. Pugno, and et al., Nat. Mater **11**, 294 (2012).

[86]C. Lee, Q. Li, W. Kalb, X.-Z. Liu, H. Berger, R. W. Carpick, and J. Hone, Science **328**, 76 (2010).

[87]W. Gao and A. Tkatchenko, Physical Review Letters **114**, 096101 (2015).

[88]J. H. Kim, J. H. Jeong, N. Kim, R. Joshi, and G.-H. Lee, J. Phys. D: Appl. Phys. **52**, 083001 (2018).

[89]D. G. Papageorgiou, Z. Li, M. Liu, I. A. Kinloch, and R. J. Young, Nanoscale **12**, 2228 (2020).

[90]H. Zhan, D. Guo, and G. Xie, Nanoscale **11**, 13181 (2019).

[91]C. Jin, A. Davoodabadi, J. Li, Y. Wang, and T. Singler, Journal of the Mechanics and Physics of Solids **100**, 85 (2017).

[92]M. W. Pruessner, T. T. King, D. P. Kelly, R. Grover, L. C. Calhoun, and R. Ghodssi, Sensors and Actuators A: Physical **105**, 190 (2003).

[93]J. Han, N. M. Pugno, and S. Ryu, Nanoscale **7**, 15672 (2015).

[94]R. J. T. Nicholl, H. J. Conley, N. V. Lavrik, I. Vlassiouk, Y. S. Puzyrev, V. P. Sreenivas, S. T. Pantelides, and K. I. Bolotin, Nature Communications **6**, 8789 (2015).

[95]C. S. Ruiz-Vargas, H. L. Zhuang, P. Y. Huang, A. M. van der Zande, S. Garg, P. L. McEuen, D. A. Muller, R. G. Hennig, and J. Park, Nano Lett. **11**, 2259 (2011).

[96]T. Cui, S. Mukherjee, P. M. Sudeep, G. Colas, F. Najafi, J. Tam, P. M. Ajayan, C. V. Singh, Y. Sun, and T. Filleter, Nature Materials **19**, 405 (2020).

[97]X. Zhao, D. G. Papageorgiou, L. Zhu, F. Ding, and R. J. Young, Nanoscale **11**, 14339 (2019).

[98]K. Cao, S. Feng, Y. Han, L. Gao, T. Hue Ly, Z. Xu, and Y. Lu, Nature Communications **11**, 284 (2020).

[99]G. Wang, Z. Dai, Y. Wang, P. Tan, L. Liu, Z. Xu, Y. Wei, R. Huang, and Z. Zhang, Phys. Rev. Lett. **119**, 036101 (2017).

[100]G. Tsoukleri, J. Parthenios, K. Papagelis, R. Jalil, A. C. Ferrari, A. K. Geim, K. S. Novoselov, and C. Galiotis, Small **5**, 2397 (2009).

[101]Z. Li, R. J. Young, D. G. Papageorgiou, I. A. Kinloch, X. Zhao, C. Yang, and S. Hao, 2D Mater. **6**, 045026 (2019).

[102]A. C. Ferrari, J. C. Meyer, V. Scardaci, C. Casiraghi, M. Lazzeri, F. Mauri, S. Piscanec, D. Jiang, K. S. Novoselov, S. Roth, and et al., Phys Rev Lett **97** (2006), 10.1103/physrevlett.97.187401.

[103]Y. Shin, M. Lozada Hidalgo, J. L. Sambricio Garcia, I. Grigorieva, A. Geim, and C. Casiraghi, Appl Phys Lett **108**, 221907 (2016).

[104]C. Neumann, S. Reichardt, P. Venezuela, M. Drögeler, L. Banszerus, M. Schmitz, K. Watanabe, T. Taniguchi, F. Mauri, B. Beschoten, *et al.*, Nature Communications **6**, 1 (2015).

[105]L. Gong, R. J. Young, I. A. Kinloch, I. Riaz, R. Jalil, and K. S. Novoselov, ACS Nano **6**, 2086 (2012).

[106]J. Zabel, R. R. Nair, A. Ott, T. Georgiou, A. K. Geim, K. S. Novoselov, and C. Casiraghi, Nano Letters **12**, 617 (2012).

[107]J.-B. Wu, Z.-X. Hu, X. Zhang, W.-P. Han, Y. Lu, W. Shi, X.-F. Qiao, M. Ijiäs, S. Milana, W. Ji, A. C. Ferrari, and P.-H. Tan, ACS Nano **9**, 7440 (2015).

[108]H. Kataura, Y. Kumazawa, Y. Maniwa, I. Umezu, S. Suzuki, Y. Ohtsuka, and Y. Achiba, Synth Met **103**, 2555 (1999).

[109]I. Brihuega, P. Mallet, H. González-Herrero, G. Trambly de Laissardière, M. M. Ugeda, L. Magaud, J. M. Gómez-Rodríguez, F. Ynduráin, and J.-Y. Veuillen, Physical Review Letters **109** (2012), 10.1103/PhysRevLett.109.196802.

[110]P. Zhang, L. Ma, F. Fan, Z. Zeng, C. Peng, P. E. Loya, Z. Liu, Y. Gong, J. Zhang, X. Zhang, P. M. Ajayan, T. Zhu, and J. Lou, Nature Communications **5**, 3782 (2014).

[111]M. Fujihara, R. Inoue, R. Kurita, T. Taniuchi, Y. Motoyui, S. Shin, F. Komori, Y. Maniwa, H. Shinohara, and Y. Miyata, ACS Nano **9**, 9027 (2015).

[112]K. Kim, V. I. Artyukhov, W. Regan, Y. Liu, M. F. Crommie, B. I. Yakobson, and A. Zettl, Nano Lett. **12**, 293 (2012).

[113]J. Williams, International Journal of Fracture **87**, 265 (1997).

[114]S. P. Koenig, N. G. Boddeti, M. L. Dunn, and J. S. Bunch, Nature Nanotechnology **6**, 543 (2011).

[115]N. G. Boddeti, S. P. Koenig, R. Long, J. Xiao, J. S. Bunch, and M. L. Dunn, Journal of Applied Mechanics **80** (2013), 10.1115/1.4024255.

[116]J. Hass, F. Varchon, J. E. Millán-Otoya, M. Sprinkle, N. Sharma, W. A. de Heer, C. Berger, P. N. First, L. Magaud, and E. H. Conrad, Phys. Rev. Lett. **100**, 125504 (2008).

[117]B. A. Auld, *Acoustic Fields and Waves in Solids* (Wiley, 1973).

[118]K. H. Michel and B. Verberck, Phys. Status Solidi B **245**, 2177 (2008).

[119]F. Memarian, A. Fereidoon, and M. Darvish Ganji, Superlattices and Microstructures **85**, 348 (2015).

[120]B. D. Jensen, K. E. Wise, and G. M. Odegard, J. Phys. Chem. A **119**, 9710 (2015).

[121]G. Kalosakas, N. N. Lathiotakis, C. Galiotis, and K. Papagelis, Journal of Applied Physics **113**, 134307 (2013).

[122]I. V. Lebedeva, A. S. Minkin, A. M. Popov, and A. A. Knizhnik, Physica E: Low-dimensional Systems and Nanostructures **108**, 326 (2019).

[123]G. Gui, J. Li, and J. Zhong, Phys. Rev. B **78**, 075435 (2008).

[124]F. Liu, P. Ming, and J. Li, Phys. Rev. B **76**, 064120 (2007).

[125]L. Zhou and G. Cao, Phys. Chem. Chem. Phys. **18**, 1657 (2016).

[126]J. Pellicer-Porres, A. Segura, C. Ferrer, V. Muñoz, A. San Miguel, A. Polian, J. P. Itié, M. Gauthier, and S. Pascarelli, Phys. Rev. B **65**, 174103 (2002).

[127]S. Deng and V. Berry, Materials Today **19**, 197 (2016).

[128]J. C. Meyer, A. K. Geim, M. I. Katsnelson, K. S. Novoselov, T. J. Booth, and S. Roth, Nature **446**, 60 (2007).

[129]J. S. Bunch, S. S. Verbridge, J. S. Alden, A. M. van der Zande, J. M. Parpia, H. G. Craighead, and P. L. McEuen, Nano Letters **8**, 2458 (2008).

[130]Z. Lu and M. L. Dunn, Journal of Applied Physics **107**, 044301 (2010).

[131]Z. Tao, J. Du, Z. Qi, K. Ni, S. Jiang, and Y. Zhu, Appl. Phys. Lett. **116**, 133101 (2020).

[132]J. Nicolle, *Etude Du Graphène Sous Pression Par Spectroscopie Raman*, Ph.D. thesis, Université Claude Bernard Lyon 1 (2011).

[133]A. Forestier, F. Balima, C. Bousige, G. d. S. Pinheiro, R. Fulcrand, M. Kalbáč, D. Machon, and A. San-Miguel, J. Phys. Chem. C **124**, 11193 (2020).

[134]L. G. P. Martins, M. J. S. Matos, A. R. Paschoal, P. T. C. Freire, N. F. Andrade, A. L. Aguiar, J. Kong, B. R. A. Neves, A. B. de Oliveira, M. S. Mazzoni, and et al., Nat. Comm **8** (2017), 10.1038/s41467-017-00149-8.

[135]A. Das, S. Pisana, B. Chakraborty, S. Piscanec, S. K. Saha, U. V. Waghmare, K. S. Novoselov, H. R. Krishnamurthy, A. K. Geim, A. C. Ferrari, and A. K. Sood, Nature Nanotech **3**, 210 (2008).

[136]M. J. Longhurst and N. Quirke, Phys. Rev. Lett. **98**, 145503 (2007).

[137]W. Cui, T. F. T. Cerqueira, S. Botti, M. A. L. Marques, and A. San-Miguel, Phys. Chem. Chem. Phys. **18**, 19926 (2016).

[138]S. Azadi and R. E. Cohen, J. Chem. Phys. **145**, 064501 (2016).

[139]J.-U. Lee, D. Yoon, and H. Cheong, Nano Lett. **12**, 4444 (2012).

[140]D. Davidovikj, F. Alijani, S. J. Cartamil-Bueno, H. S. J. van der Zant, M. Amabili, and P. G. Steeneken, Nat Commun **8**, 1 (2017).

[141]B. Sajadi, F. Alijani, D. Davidovikj, J. H. Goosen, P. G. Steeneken, and F. van Keulen, Journal of Applied Physics **122**, 234302 (2017).

[142]B. Sajadi, S. van Hemert, B. Arash, P. Belardinelli, P. G. Steeneken, and F. Alijani, Carbon **139**, 334 (2018).

[143]P. Lambin, Appl. Sci. **4**, 282 (2014).

[144]P. Lambin, Applied Sciences **7**, 830 (2017).

[145]O. Pierre-Louis, Phys Rev E **78**, 021603 (2008).

[146]D. Machon, C. Bousige, R. Alencar, A. Torres-Dias, F. Balima, J. Nicolle, G. Pinheiro de Sousa, A. G. de Souza Filho, and A. San-Miguel, J Raman Spectrosc **49**, 121 (2018).

[147]A. Reserbat-Plantey, D. Kalita, Z. Han, L. Ferlazzo, S. Autier-Laurent, K. Komatsu, C. Li, R. Weil, A. Ralko, L. Marty, S. Guéron, N. Bendiab, H. Bouchiat, and V. Bouchiat, Nano Lett **14**, 5044 (2014).

[148]A. Forestier, *Dimensionality effects in graphene at high hydrostatic pressure*, Ph.D. thesis, Université Claude Bernard Lyon 1 (2020).

[149]R. S. Alencar, K. D. A. Saboia, D. Machon, G. Montagnac, V. Meunier, O. P. Ferreira, A. San-Miguel, and A. G. Souza Filho, Phys Rev Mater. **1** (2017), 10.1103/physrevmaterials.1.024002.

[150]D. Y. Usachov, V. Y. Davydov, V. S. Levitskii, V. O. Shevelev, D. Marchenko, B. V. Senkovskiy, O. Y. Vilkov, A. G. Rybkin, L. V. Yashina, E. V. Chulkov, I. Y. Sklyadneva, R. Heid, K.-P. Bohnen, C. Laubschat, and D. V. Vyalikh, ACS Nano **11**, 6336 (2017).

[151]N. Bendiab, J. Renard, C. Schwarz, A. Reserbat-Plantey, L. Djevahirdjian, V. Bouchiat, J. Coraux, and L. Marty, J. Raman Spectrosc. **49**, 130 (2018).

[152]J. E. Lee, G. Ahn, J. Shim, Y. S. Lee, and S. Ryu, Nat. Comm **3**, 1024 (2012).

[153]C. Thomsen, S. Reich, and P. Ordejon, Phys Rev B **65**, 073403 (2002).

[154]W. Cui, T. F. T. Cerqueira, S. Botti, M. A. L. Marques, and A. San-Miguel, Phys Chem Chem Phys **18**, 19926 (2016).

[155]S. Klotz, J. Chervin, P. Munsch, and G. Le Marchand, J Phys Appl Phys **42**, 075413 (2009).

[156]R. J. Young, L. Gong, I. A. Kinloch, I. Riaz, R. Jalil, and K. S. Novoselov, ACS Nano **5**, 3079 (2011), pMID: 21395299.

[157]R. J. Young, I. A. Kinloch, L. Gong, and K. S. Novoselov, Composites Science and Technology **72**, 1459 (2012).

[158]F. Piazza, K. Cruz, M. Monthioux, P. Puech, and I. Gerber, Carbon **169**, 129 (2020).

[159]P. V. Bakharev, M. Huang, M. Saxena, S. W. Lee, S. H. Joo, S. O. Park, J. Dong, D. C. Camacho-Mojica, S. Jin, Y. Kwon, *et al.*, Nature Nanotechnology **15**, 59 (2020).

[160]J. W. Suk, R. D. Piner, J. An, and R. S. Ruoff, ACS Nano **4**, 6557 (2010).

[161]L. A. Chernozatonskii, P. B. Sorokin, A. A. Kuzubov, B. P. Sorokin, A. G. Kvashnin, D. G. Kvashnin, P. V. Avramov, and B. I. Yakobson, Journal of Physical Chemistry C **115**, 132 (2011).

[162]A. R. Khoei and M. S. Khorrami, Fullerenes, Nanotubes and Carbon Nanostructures **24**, 594 (2016).

[163]I. Razado-Colambo, J. Avila, D. Vignaud, S. Godey, X. Wallart, D. P. Woodruff, and M. C. Asensio, Scientific Reports **8**, 10190 (2018).

[164]F. Varchon, R. Feng, J. Hass, X. Li, B. N. Nguyen, C. Naud, P. Mallet, J.-Y. Veuillen, C. Berger, E. H. Conrad, and L. Magaud, Phys. Rev. Lett. **99**, 126805 (2007).

[165]S. Reich and C. Thomsen, Philosophical Transactions of the Royal Society of London. Series A: Mathematical, Physical and Engineering Sciences **362**, 2271 (2004).

[166]M. Huang, H. Yan, C. Chen, D. Song, T. F. Heinz, and J. Hone, Proceedings of the National Academy of Sciences **106**, 7304 (2009).

[167]Y. W. Sun, D. Holec, and D. J. Dunstan, Physical Review B **92** (2015), 10.1103/PhysRevB.92.094108.

[168]R. A. Friedel and G. L. Carlson, J. Phys. Chem. **75**, 1149 (1971).

[169]S. Piscanec, M. Lazzeri, J. Robertson, A. C. Ferrari, and F. Mauri, Physical Review B **75**, 035427 (2007).

[170]J. Zabel, R. R. Nair, A. Ott, T. Georgiou, A. K. Geim, K. S. Novoselov, and C. Casiraghi, Nano Lett **12**, 617 (2012).

[171]V. N. Popov, New J. Phys. **6**, 17 (2004).

[172]J. Maultzsch, H. Telg, S. Reich, and C. Thomsen, Phys. Rev. B **72**, 205438 (2005).

[173]G. Mahan, Physical Review B **65**, 235402 (2002).

[174]S. M. Bachilo, M. S. Strano, C. Kittrell, R. H. Hauge, R. E. Smalley, and R. B. Weisman, Science **298**, 2361 (2002).

[175]I. C. Gerber, P. Puech, A. Gannouni, and W. Bacsa, Physical Review B **79**, 075423 (2009).

[176]Y. Shen and D. Zerulla, Phys. Rev. B **95**, 205434 (2017).

[177]A. J. Ghandour, D. J. Dunstan, and A. Sapelkin, J. Raman Spectrosc. **42**, 1611 (2011).

[178]J. E. Proctor, M. P. Halsall, A. Ghandour, and D. J. Dunstan, Journal of Physics and Chemistry of Solids **67**, 2468 (2006).

[179]C. Thomsen, S. Reich, H. Jantoljak, I. Loa, K. Syassen, M. Burghard, G. Duesberg, and S. Roth, Applied Physics A: Materials Science & Processing **69**, 309 (1999).

[180]D. Christofilos, J. Arvanitidis, C. Tzampazis, K. Papagelis, T. Takenobu, Y. Iwasa, H. Kataura, C. Lioutas, S. Ves, and G. Kourouklis, Diamond and Related Materials **15**, 1075 (2006).

[181]P. Djondjorov, V. Vassilev, and I. Mladenov, International Journal of Mechanical Sciences **53**, 355 (2011).

[182]V. M. Vassilev, P. A. Djondjorov, and I. M. Mladenov, Journal of Applied Physics **117**, 196101 (2015).

[183]J. A. Elliott, J. K. W. Sandler, A. H. Windle, R. J. Young, and M. S. P. Shaffer, Phys. Rev. Lett. **92**, 095501 (2004).

[184]N. Wang, Z.-K. Tang, G.-D. Li, and J. Chen, Nature **408**, 50 (2000).

[185]H. R. Barzegar, A. Yan, S. Coh, E. Gracia-Espino, C. Ojeda-Aristizabal, G. Dunn, M. L. Cohen, S. G. Louie, T. Wågberg, and A. Zettl, Nano Research **10**, 1942 (2017).

[186]A. Impellizzeri, P. Briddon, and C. Ewels, Physical Review B **100**, 115410 (2019).

[187]R. R. Del Grande, A. F. Fonseca, and R. B. Capaz, Carbon **159**, 161 (2020).

[188]A. Barboza, H. Chacham, and B. Neves, Physical Review Letters **102**, 025501 (2009).

[189]T. C. Hirschmann, P. T. Araujo, H. Muramatsu, J. F. Rodriguez-Nieva, M. Seifert, K. Nielsch, Y. A. Kim, and M. S. Dresselhaus, ACS Nano **8**, 1330 (2014).

[190]A. Aguiar, E. Barros, R. Capaz, A. Souza Filho, P. Freire, J. M. Filho, D. Machon, C. Caillier, Y. Kim, H. Muramatsu, M. Endo, and A. San-Miguel, J. Phys. Chem. C **115**, 5378 (2011).

[191]P. Puech, H. Hubel, D. J. Dunstan, R. Bacsa, C. Laurent, and W. Bacsa, Physical Review Letters **93**, 095506 (2004).

[192]J. González, C. Power, E. Belandria, J. Jorge, F. Gonzalez-Jimenez, M. Millot, S. Nanot, J. M. Broto, and E. Flahaut, High Pressure Research **28**, 577 (2008).

[193]A. J. Ghandour, I. F. Crowe, J. E. Proctor, Y. W. Sun, M. P. Halsall, I. Hernandez, A. Sapelkin, and D. J. Dunstan, Phys. Rev. B **87**, 085416 (2013).

[194]P. N. Keating, Phys. Rev. **145**, 637 (1966).

[195]J. Maultzsch, S. Reich, C. Thomsen, H. Requardt, and P. Ordejón, Physical Review Letters **92**, 075501 (2004).

[196]A. Lajevardipour, M. Neek-Amal, and F. M. Peeters, J. Phys.: Condens. Matter **24**, 175303 (2012), publisher: IOP Publishing.

[197]D. L. Nika and A. A. Balandin, J. Phys.: Condens. Matter **24**, 233203 (2012).

[198]D. W. Brenner, O. A. Shenderova, J. A. Harrison, S. J. Stuart, B. Ni, and S. B. Sinnott, Journal of Physics: Condensed Matter **14**, 783 (2002).

[199]S. G. Srinivasan, A. C. Van Duin, and P. Ganesh, The Journal of Physical Chemistry A **119**, 571 (2015).

[200]W. Duan, Q. Wang, K. M. Liew, and X. He, Carbon **45**, 1769 (2007).

[201]S. Reich, J. Maultzsch, C. Thomsen, and P. Ordejon, Physical Review B **66**, 035412 (2002).